Chapter 4 and 5
Crystalline state and crystallization

Regular and irregular chains

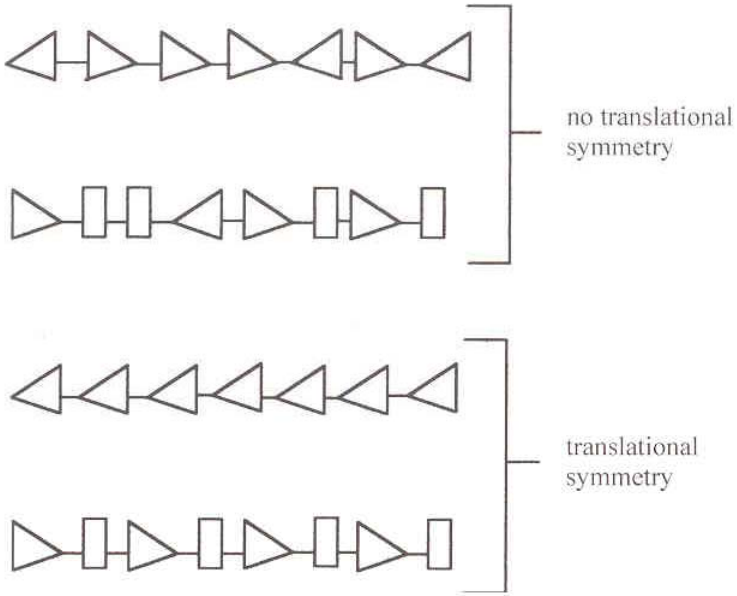

Fig. 4.1 Schematic representations of chains with and without translational symmetry. The various shapes represent different chemical groups. True translational symmetry would require the two lower chains to extend to infinity, repeating regularly as shown.

-arrangements, ex. head-to-head or head-to-tail

-tacticity

ex) vinyl polymers ....

PVC vs. PVOH

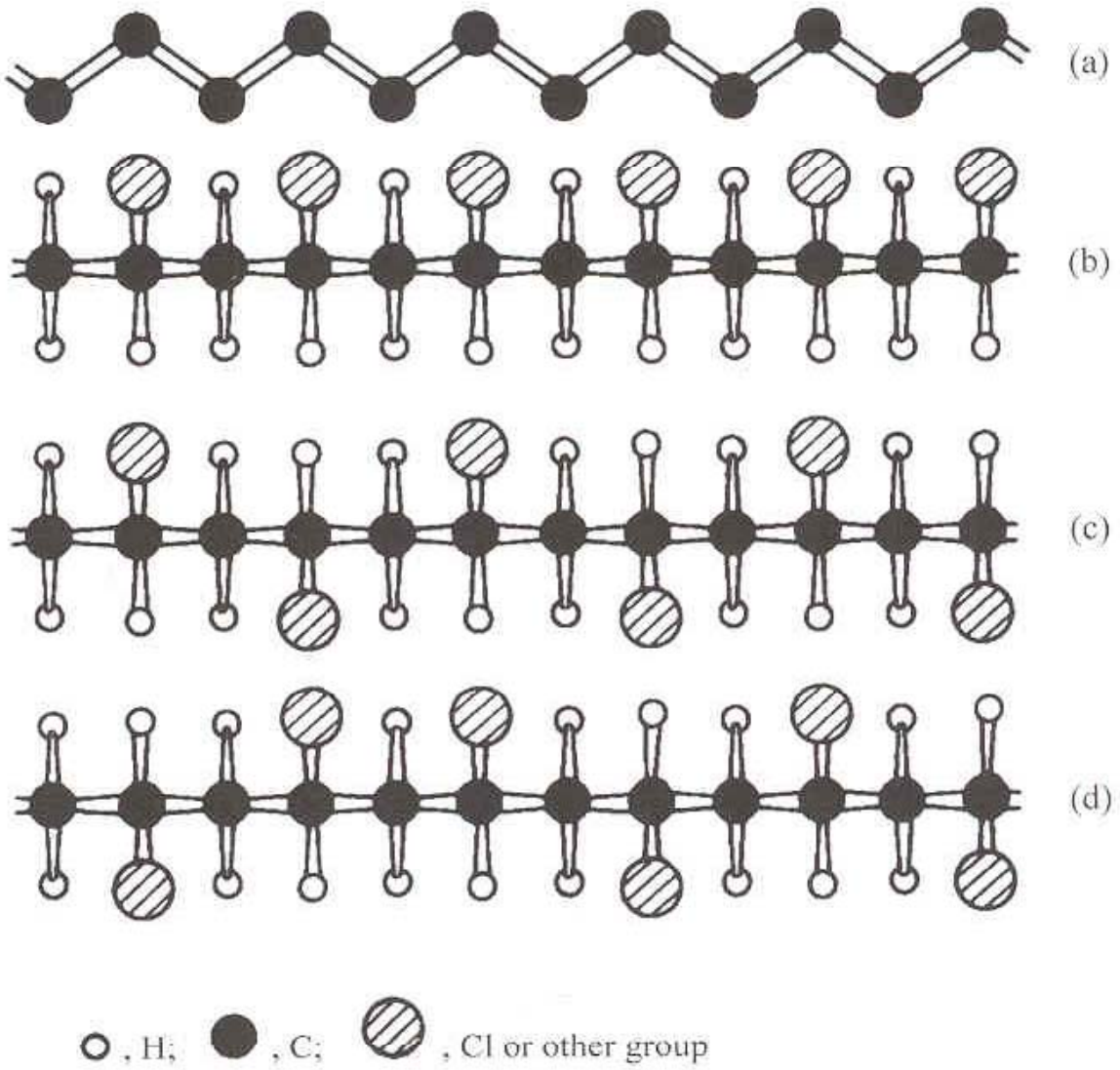

Fig. 4.2 Imagined planar zigzag conformations of vinyl polymers: (a) the carbon backbone, (b) a regular isotactic configuration, (c) a regular syndiotactic configuration and (d) a random atactic configuration. The planar zigzag conformation might not be possible for the real chain because of steric hindrance. (© Cambridge University Press 1989.)

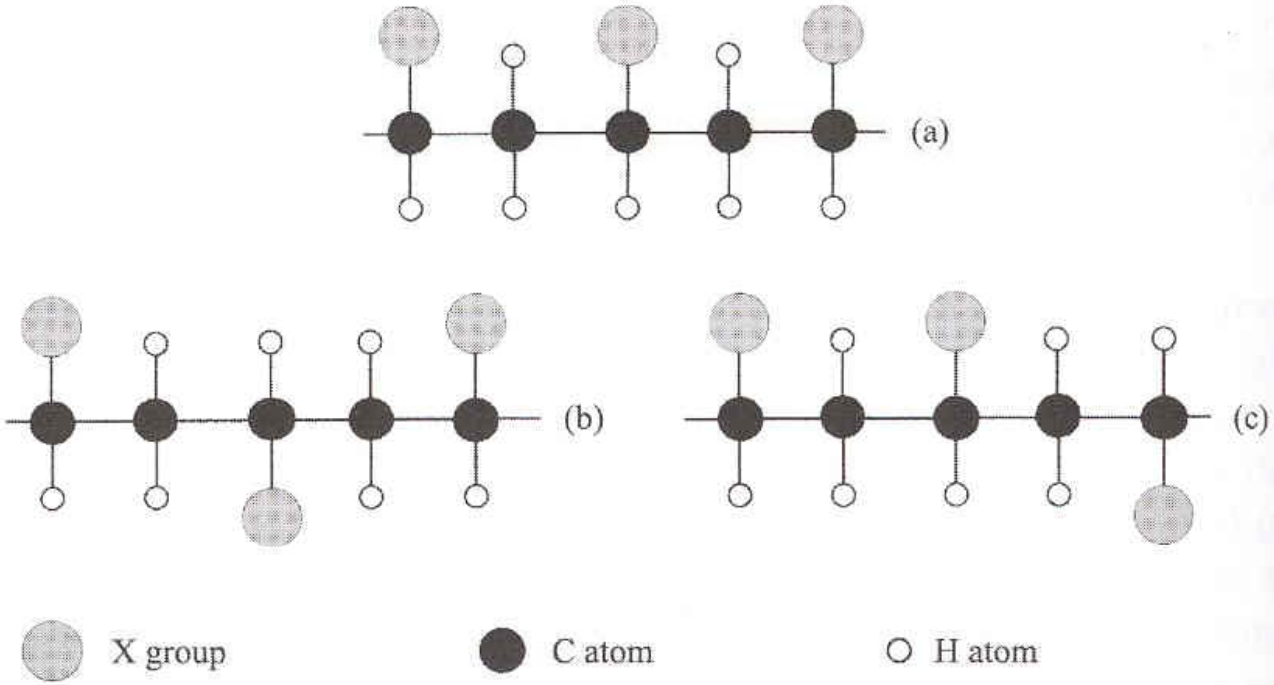

Fig. 4.4 α-carbon triads for a vinyl polymer: (a) isotactic, or mm; (b) syndiotactic, or rr, and (c) mr, where m = mesic and r = racemic.

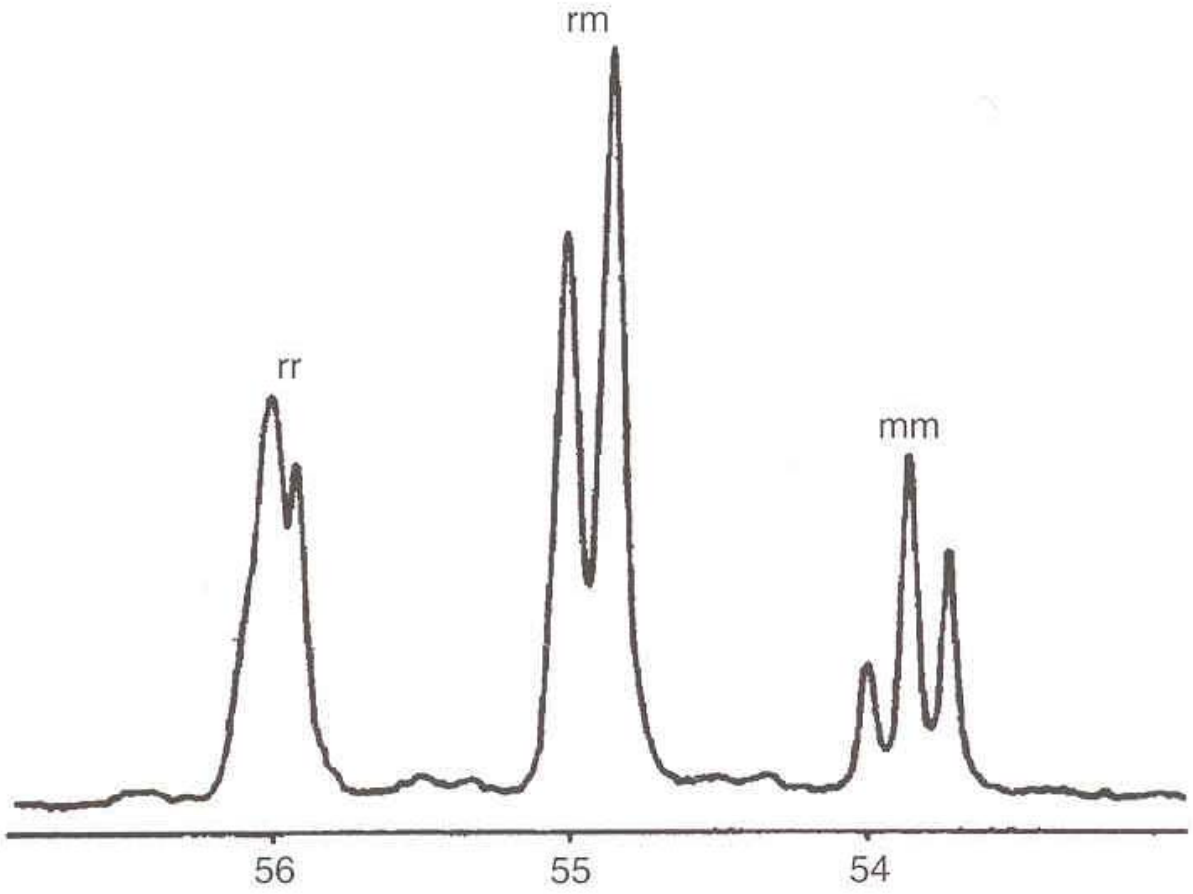

Fig. 4.5 The ^{13}C NMR spectrum in the α-carbon region for a PVC sample dissolved in *o*-dichlorobenzene. The frequencies are expressed in ppm from a standard reference frequency. (Reproduced from King, J., Bower, D. I., Maddams, W. F. and Pyszora, H., *Makromol. Chemie* **184**, 879 (1983).)

Fig. 4.6 The three possible forms of polybutadiene.

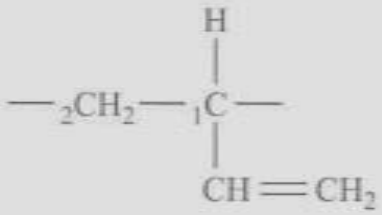

vinyl
1,2-polybutadiene

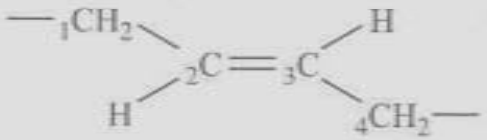

trans

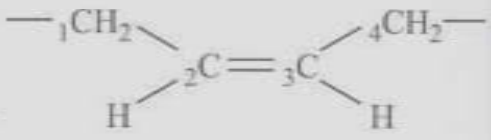

cis

1,4-polybutadiene

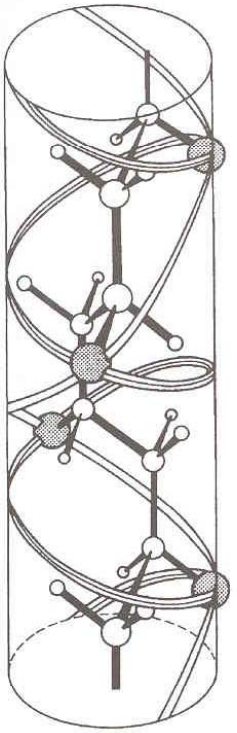

(a)

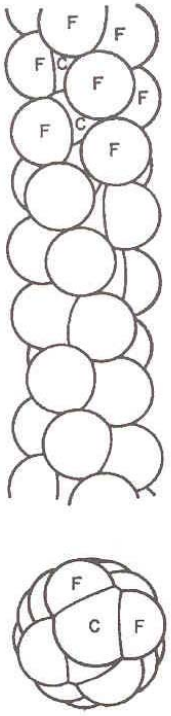

(b)

Fig. 4.7 (a) The threefold helix for an isotactic vinyl polymer. The X group of the structural unit $-(CHX-CH_2)-$ is shown shaded. The carbon backbone forms a right-handed helix and the right-handed 3_1 and the left-handed 3_2 helices are indicated by the 'ribbons'. (b) The 13_6 helix of PTFE, showing the twisted backbone, and a space-filling model viewed from the side and viewed along the chain axis. ((a) reproduced from *The Vibrational Spectroscopy of Polymers* by D. I. Bower and W. F. Maddams. © Cambridge University Press 1989; (b) reprinted by permission of Macmillan Magazines Ltd.)

Polymer crystallography

- (semi)crystalline = crystal + amorphous
- crystal = regular repeating 3-D array of atoms
- unit cell = smallest volume of repeating structure
  - depending on a, b, c, and α, β, γ

Table 7.1 Crystal systems

Systems	Axes	Axial angles	Minimum symmetry
Triclinic	$a \neq b \neq c$	$\alpha \neq \beta \neq \gamma \neq 90^\circ$	None
Monoclinic	$a \neq b \neq c$	$\alpha = \gamma = 90^\circ;\ \beta \neq 90^\circ$	One two-fold rotation axis
Orthorhombic	$a \neq b \neq c$	$\alpha = \beta = \gamma = 90^\circ$	Three perpendicular two-fold rotation axes
Tetragonal	$a = b \neq c$	$\alpha = \beta = \gamma = 90^\circ$	One four-fold rotation axis
Hexagonal	$a = b \neq c$	$\alpha = \gamma = 90^\circ;\ \beta = 120^\circ$	One six-fold rotation axis
Rhombohedral	$a = b = c$	$\alpha = \beta = \gamma \neq 90^\circ$	One three-fold rotation axis
Cubic	$a = b = c$	$\alpha = \beta = \gamma = 90^\circ$	Three four-fold rotation axes

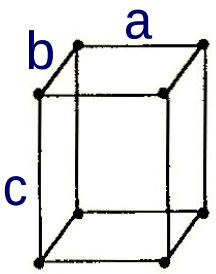

$\alpha = \angle bc$

$\beta = \angle ac$

$\gamma = \angle ab$

- polymer crystal
  - monoclinic, orthorhombic (orthogonal) popular
  - c axis is chain axis

Miller index

- The plane passing (a/h, b/k, c/l) is (hkl) plane.

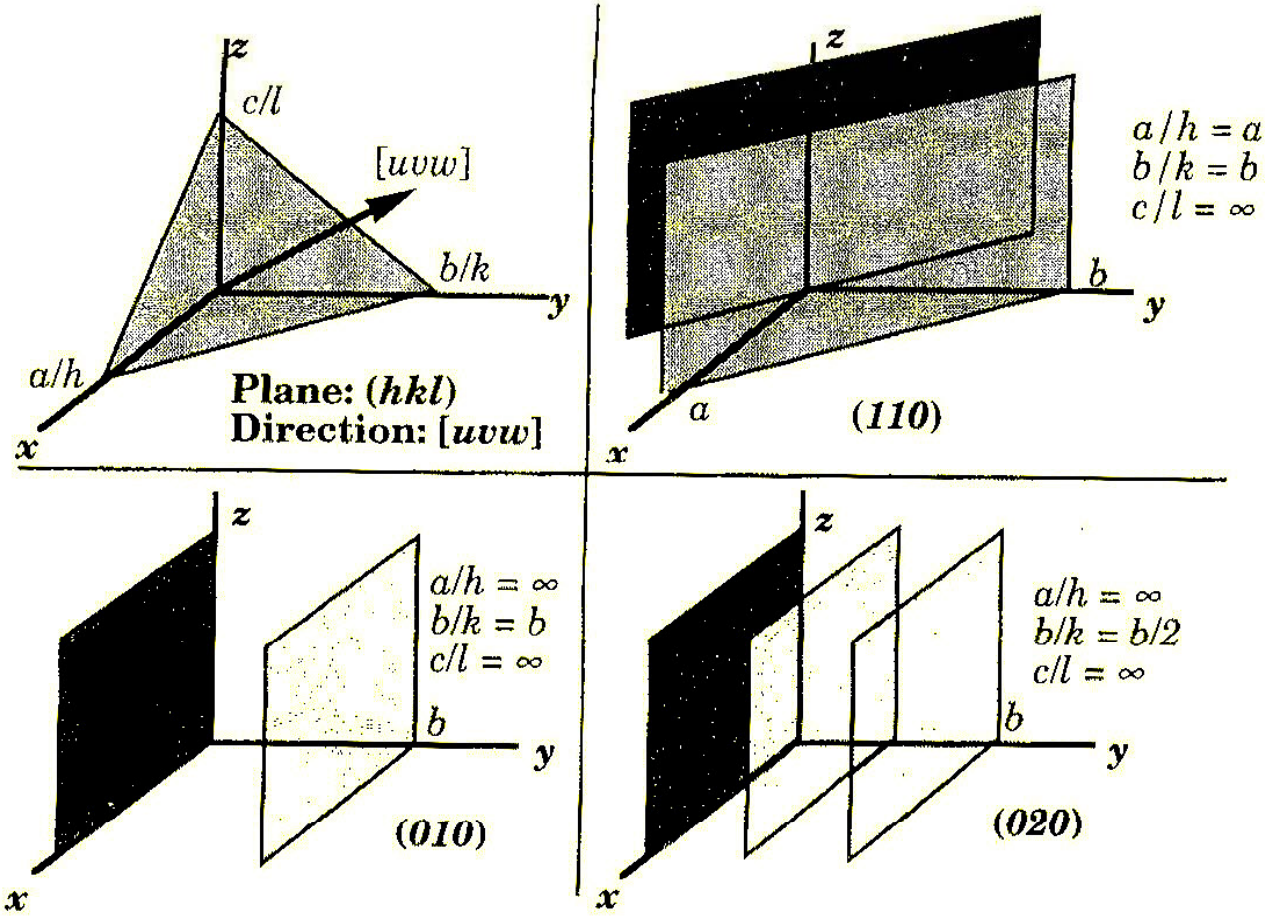

Determination of crystal structure by XRD

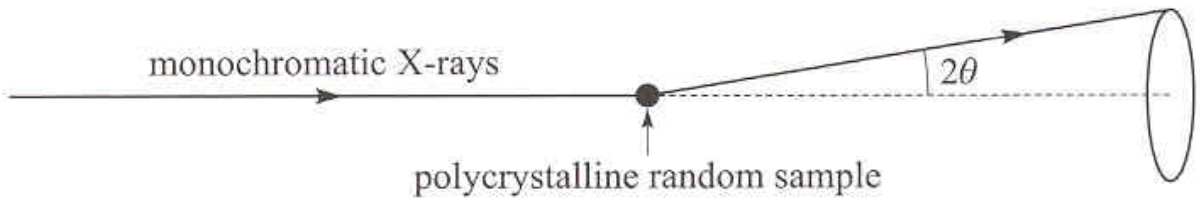

Fig. 4.8 Formation of a powder ring from a particular set of planes.

Fig. 4.9 The production of the four diffraction spots corresponding to a given set of planes for a rotation pattern: (a) the starting position, where θ_o is greater than the Bragg angle; and (b) the location of the four diffraction spots corresponding to a given set of planes.

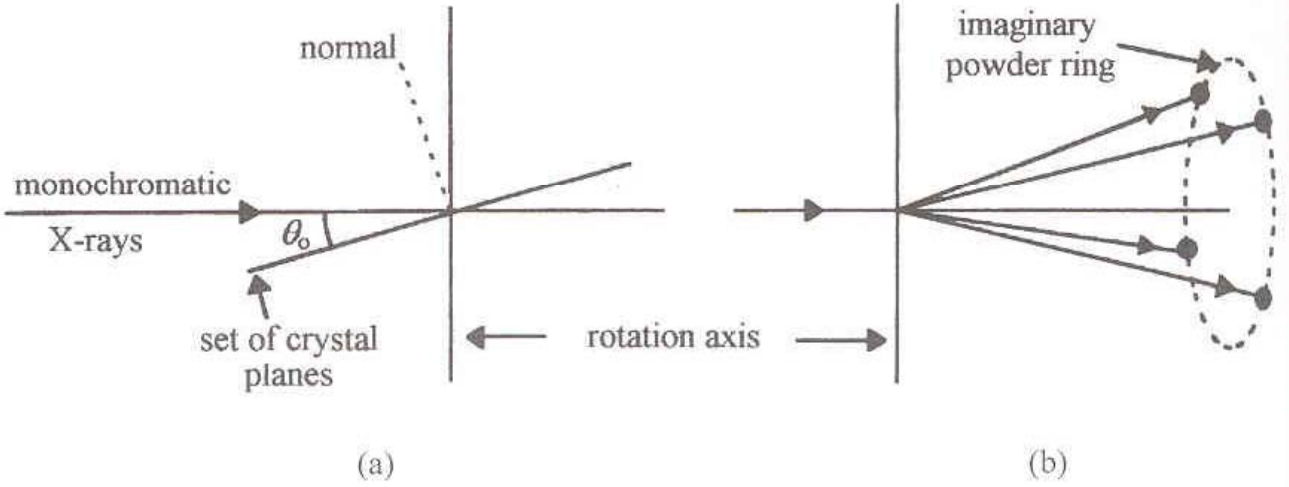

Fig. 4.11 A schematic diagram showing the relationship among layer lines, powder rings and diffraction spots in a fibre diagram. For simplicity the layer lines are shown straight and the powder rings as circles, but see the discussion in the text.

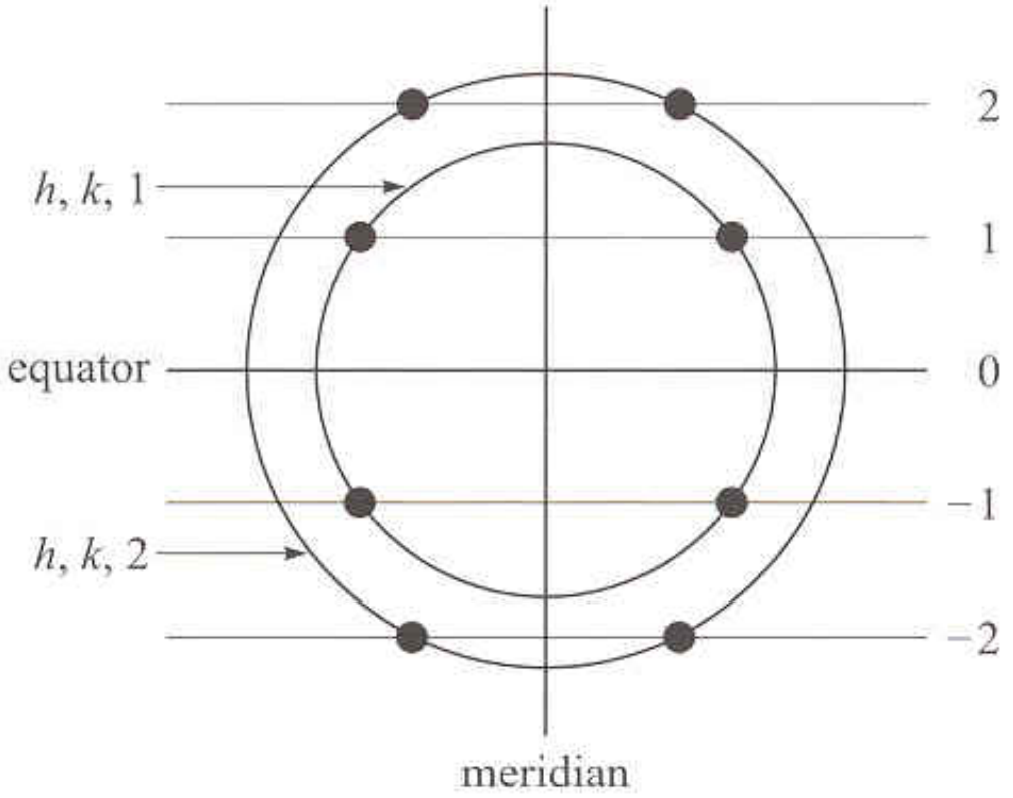

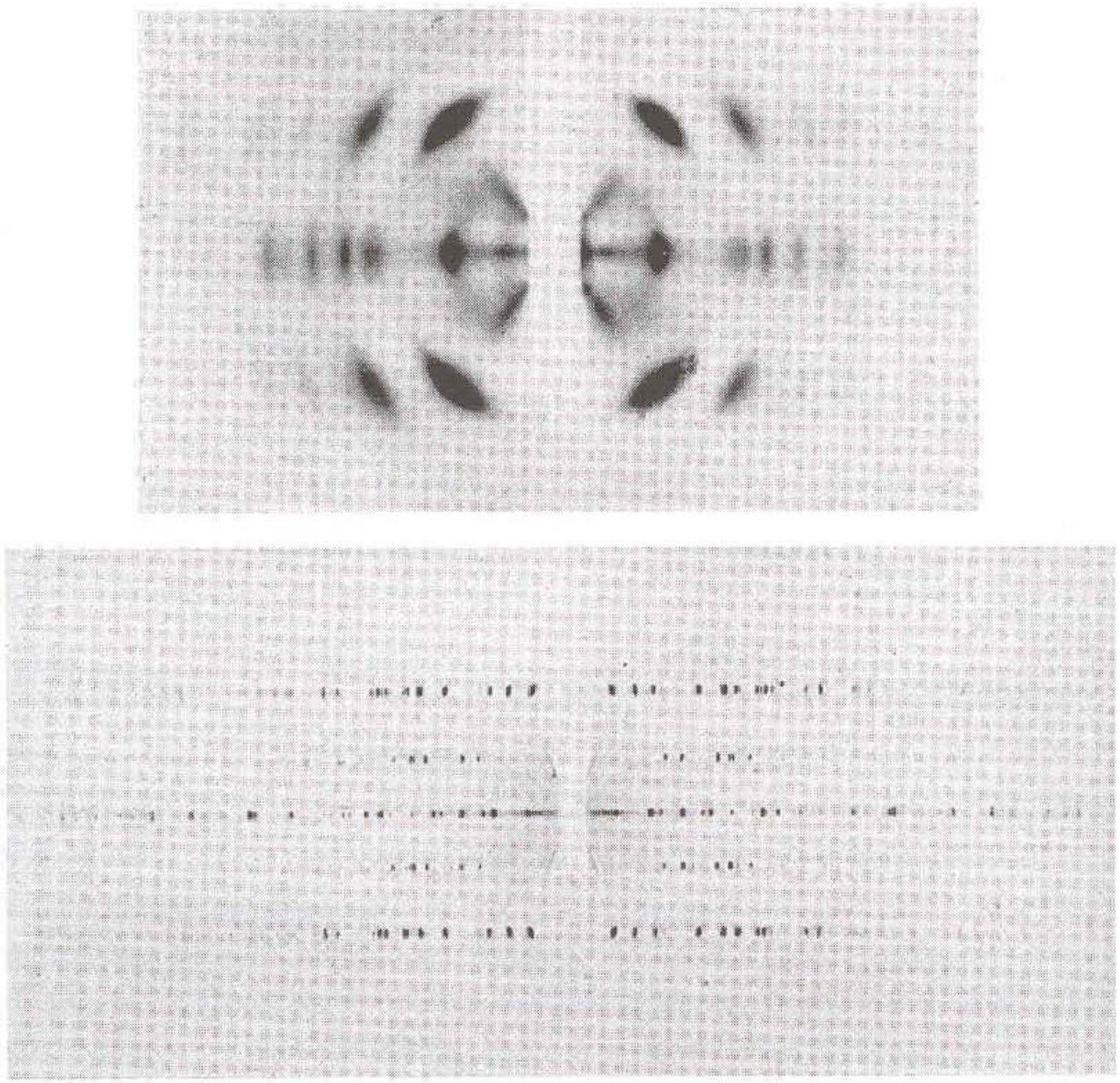

Fig. 4.12 Upper: a fibre pattern for PVDC; and lower: a rotation photograph for gypsum. (Adapted by permission of Oxford University Press.)

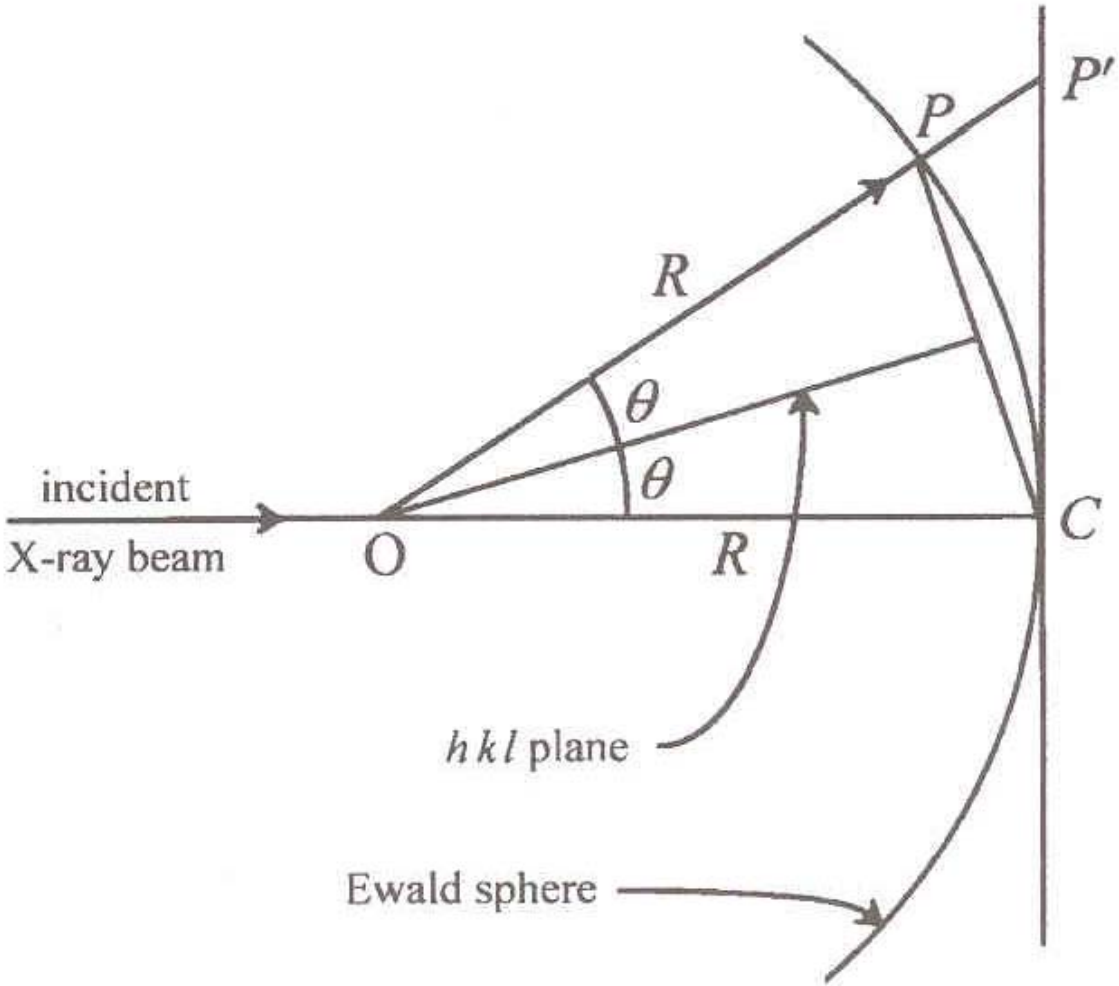

Fig. 4.13 The Ewald sphere construction for 'reflection' from a set of (*hkl*) planes. θ is the Bragg angle for this set of planes.

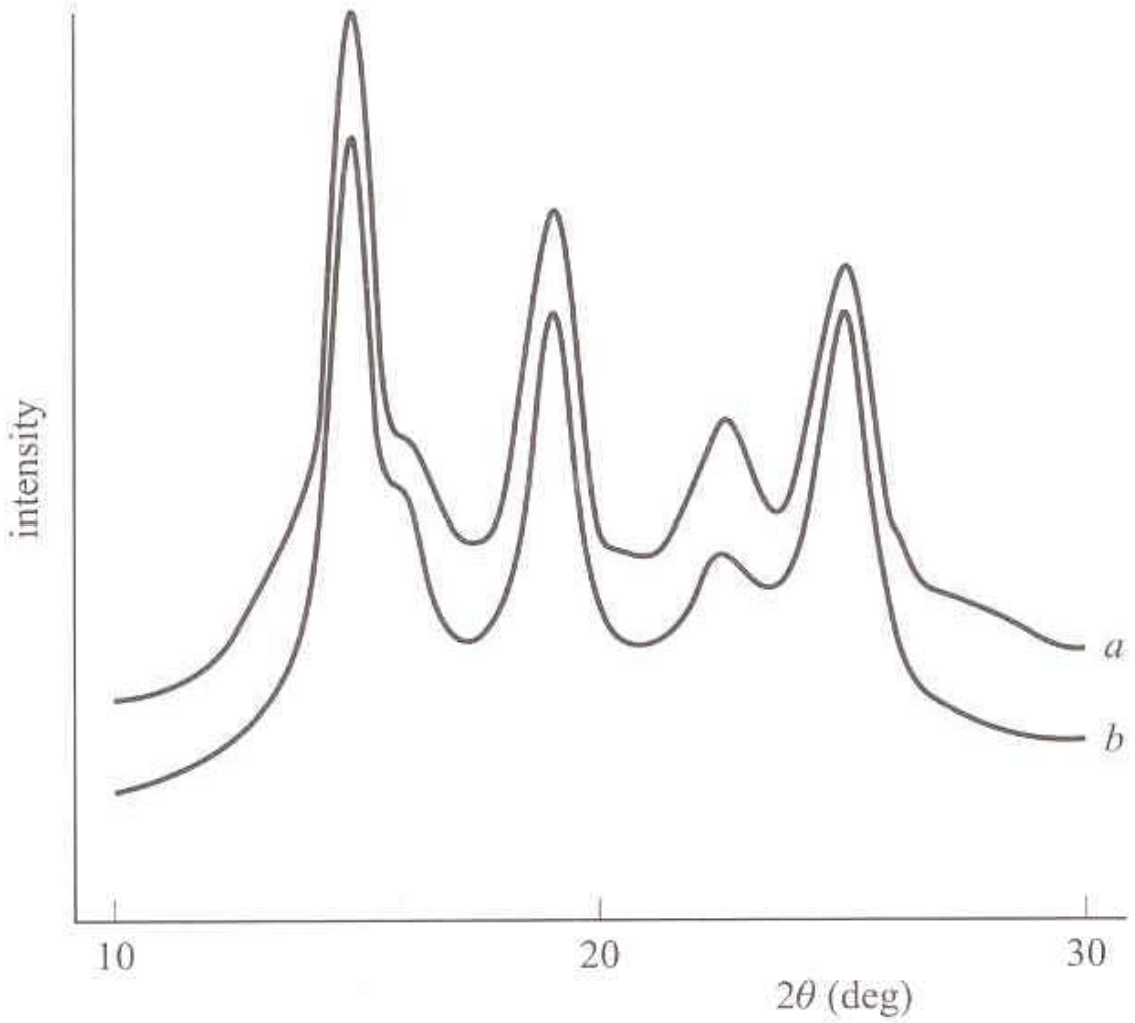

Fig. 4.14 A comparison of the observed powder ring profile for isotactic 1,4-*cis*-poly(2-methyl-1,3-pentadiene) with that calculated from the structure with minimum energy: (a) the observed profile and (b) the calculated profile, with peaks broadened to give the best fit. (Reprinted with permission from the American Chemical Society.)

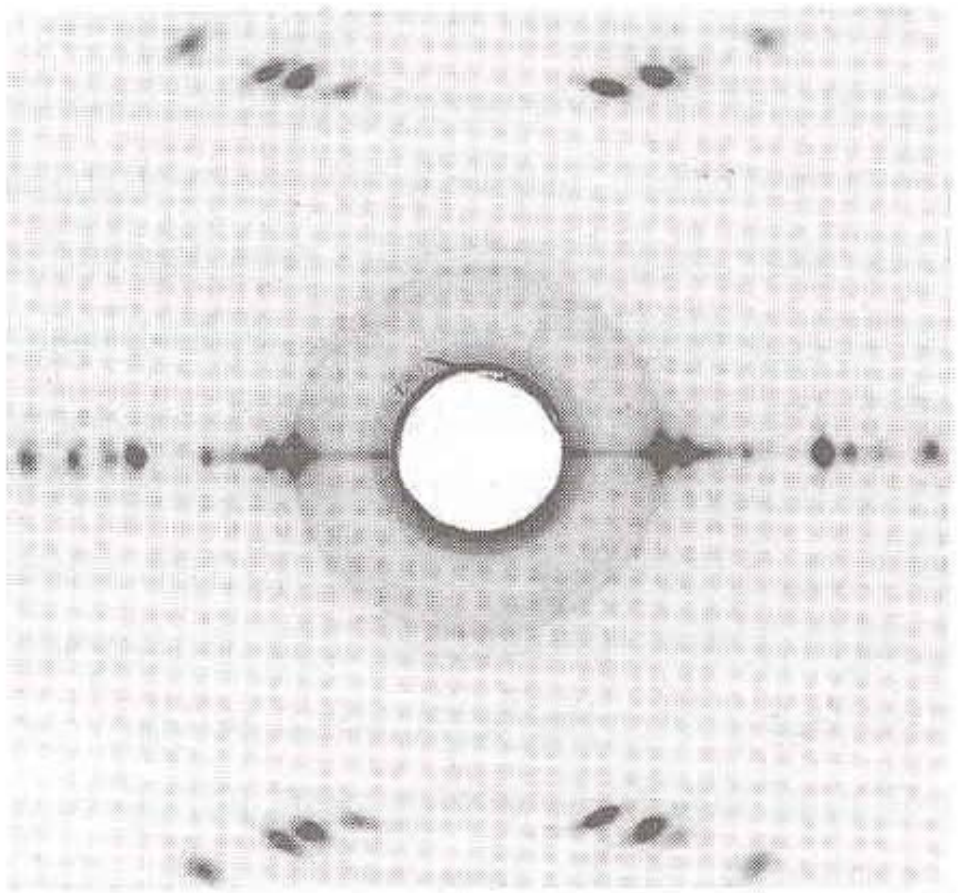

Fig. 4.15 A fibre pattern from a highly oriented sample of polyethylene. Note the two strong equatorial reflections very close together just over a third of the way out from the centre of the pattern shown. They are, from the centre outwards, the (110) and (200) reflections, respectively. (Courtesy of Dr A. P. Unwin.)

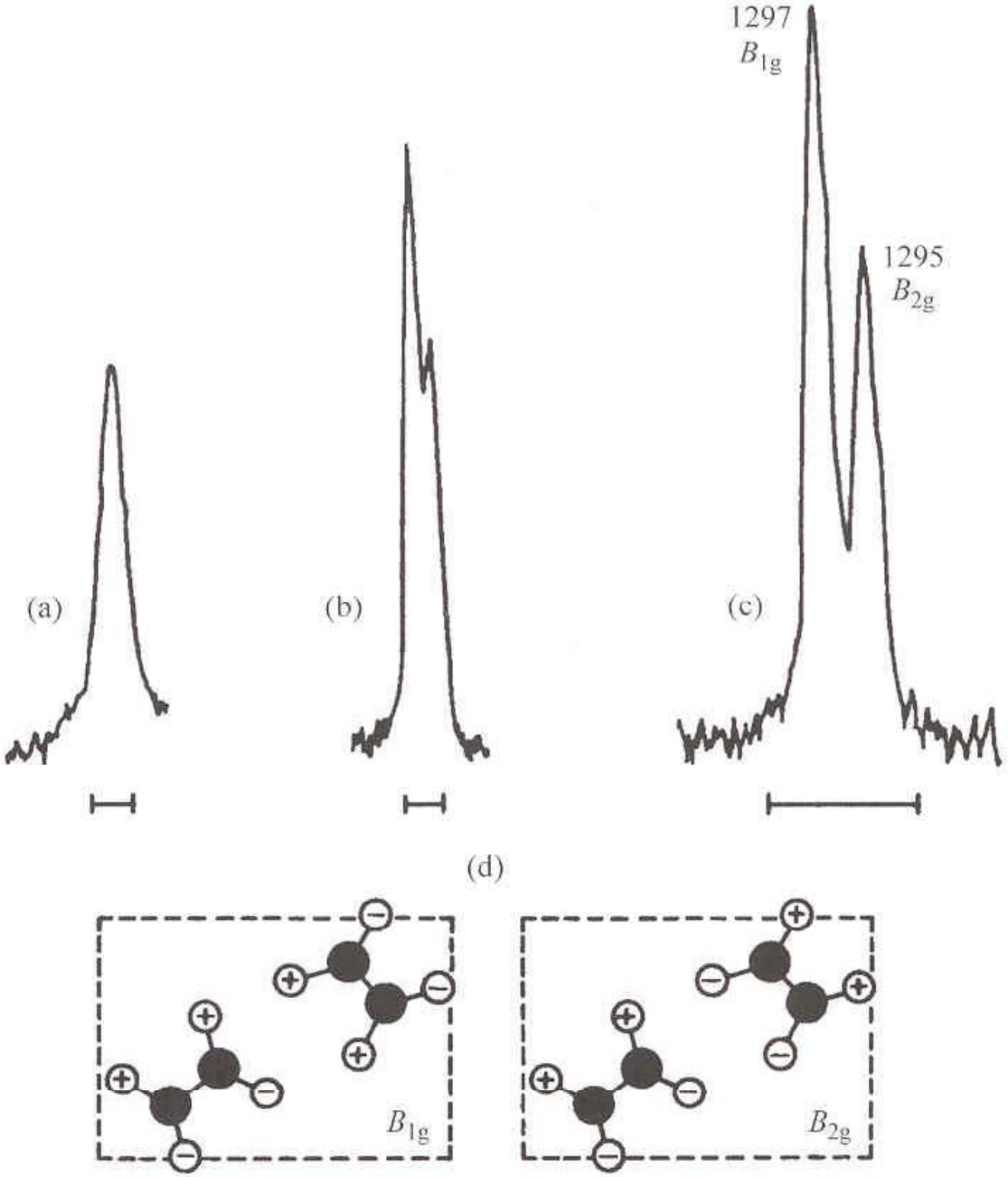

Fig. 4.16 The effect of temperature on the correlation splitting of the Raman-active CH_2-twisting doublet of polyethylene: (a) the sample at room temperature; (b) the sample at −196 °C; (c) the sample at −196 °C with increased spectral resolution and expanded wavenumber scale (⊢—⊣ indicates 5 cm^{-1} in each spectrum); and (d) forms of the vibrations. The + and − signs represent the simultaneous displacements up and down with respect to the plane of the diagram for one phase of the vibration. Only the two chains in one unit cell are shown. (Reproduced from *The Vibrational Spectroscopy of Polymers* by D. I. Bower and W. F. Maddams.)

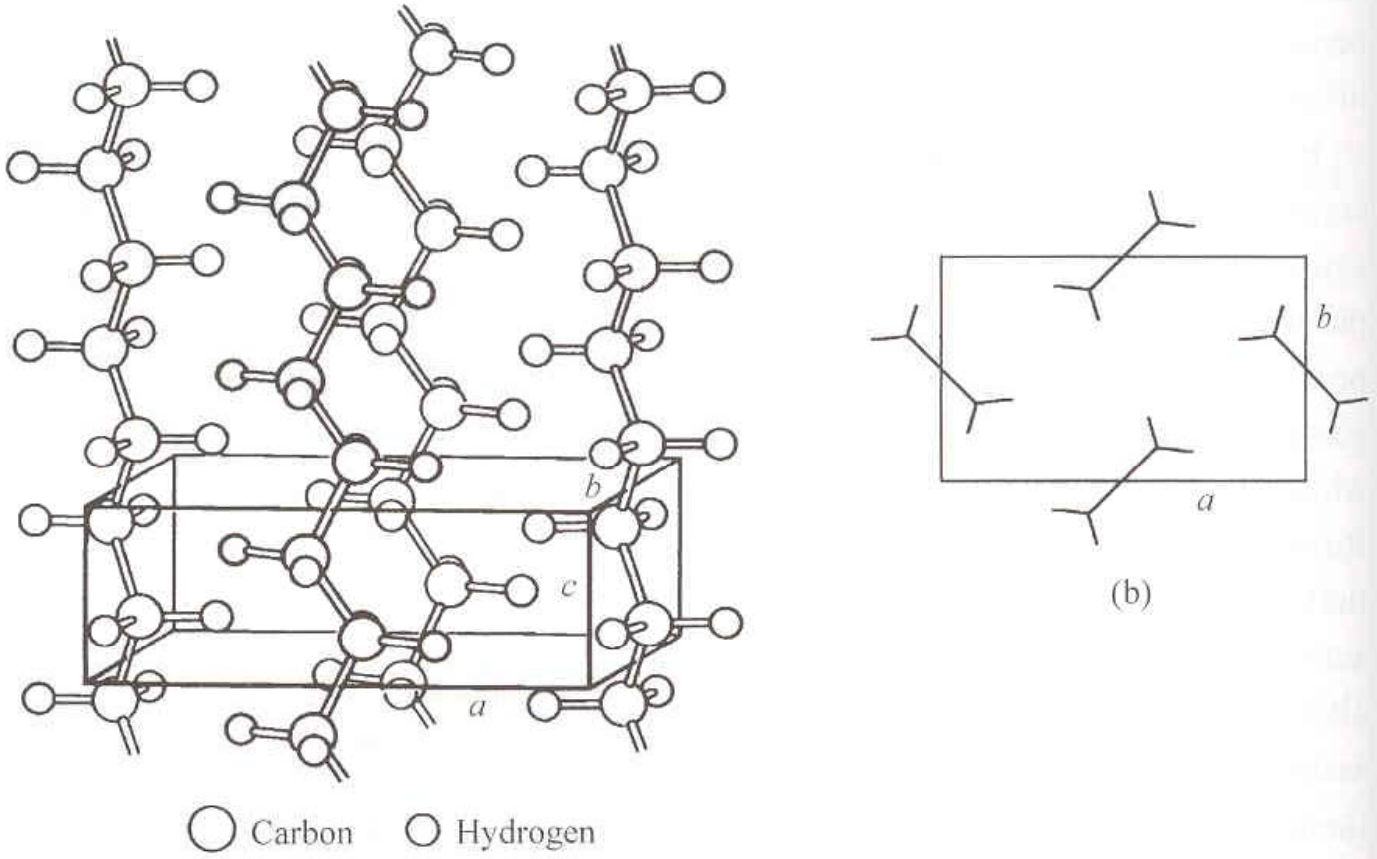

Fig. 4.17 The crystal structure of polyethylene: (a) a perspective view of the chains and the unit cell and (b) a schematic plan view looking down the *c*-axis, with only the directions of the interatomic bonds shown. ((a) Reproduced by permission of Oxford University Press.)

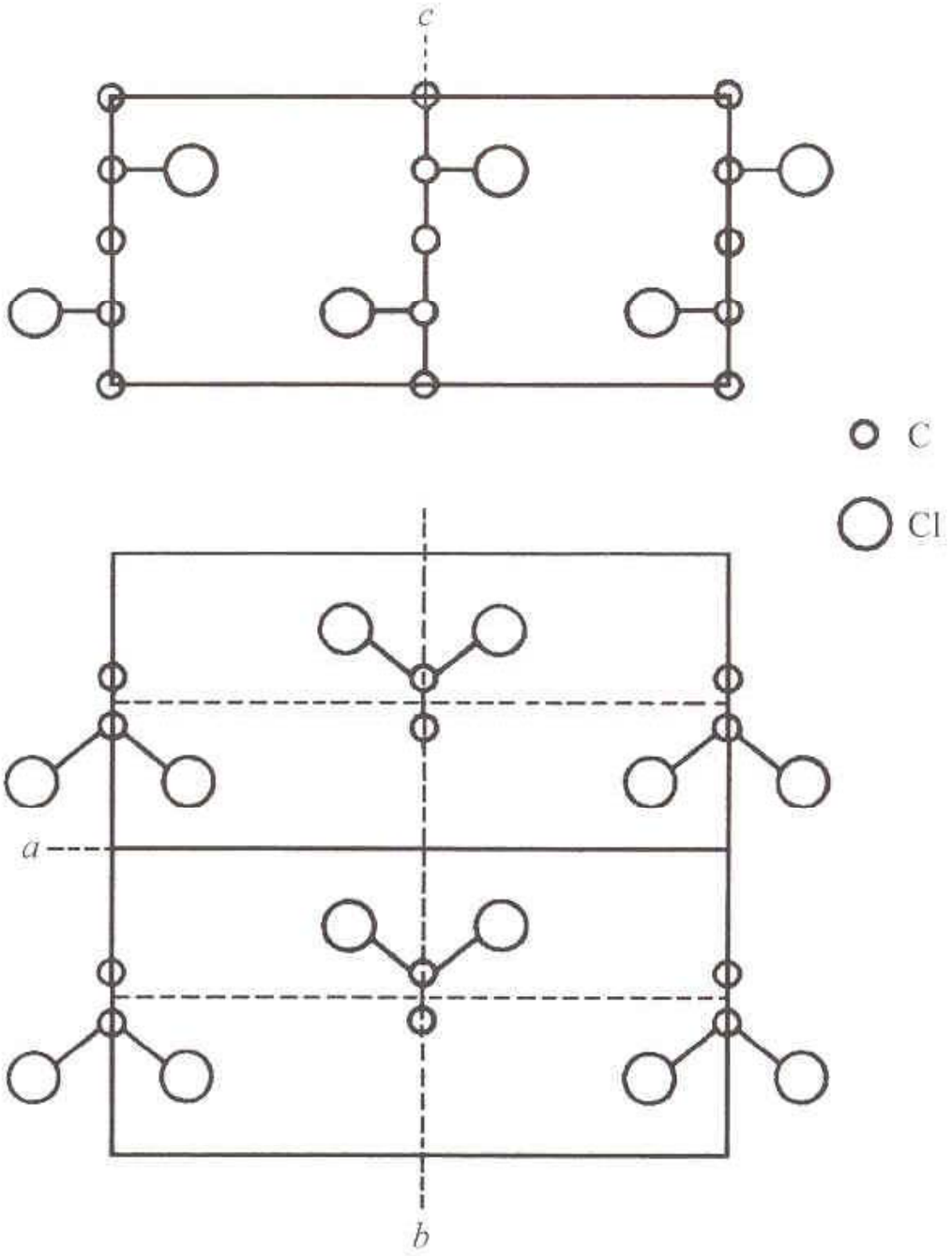

Fig. 4.18 The crystal structure of syndiotactic poly(vinyl chloride). The unit cell contains two chains. For clarity the hydrogen atoms are not shown.

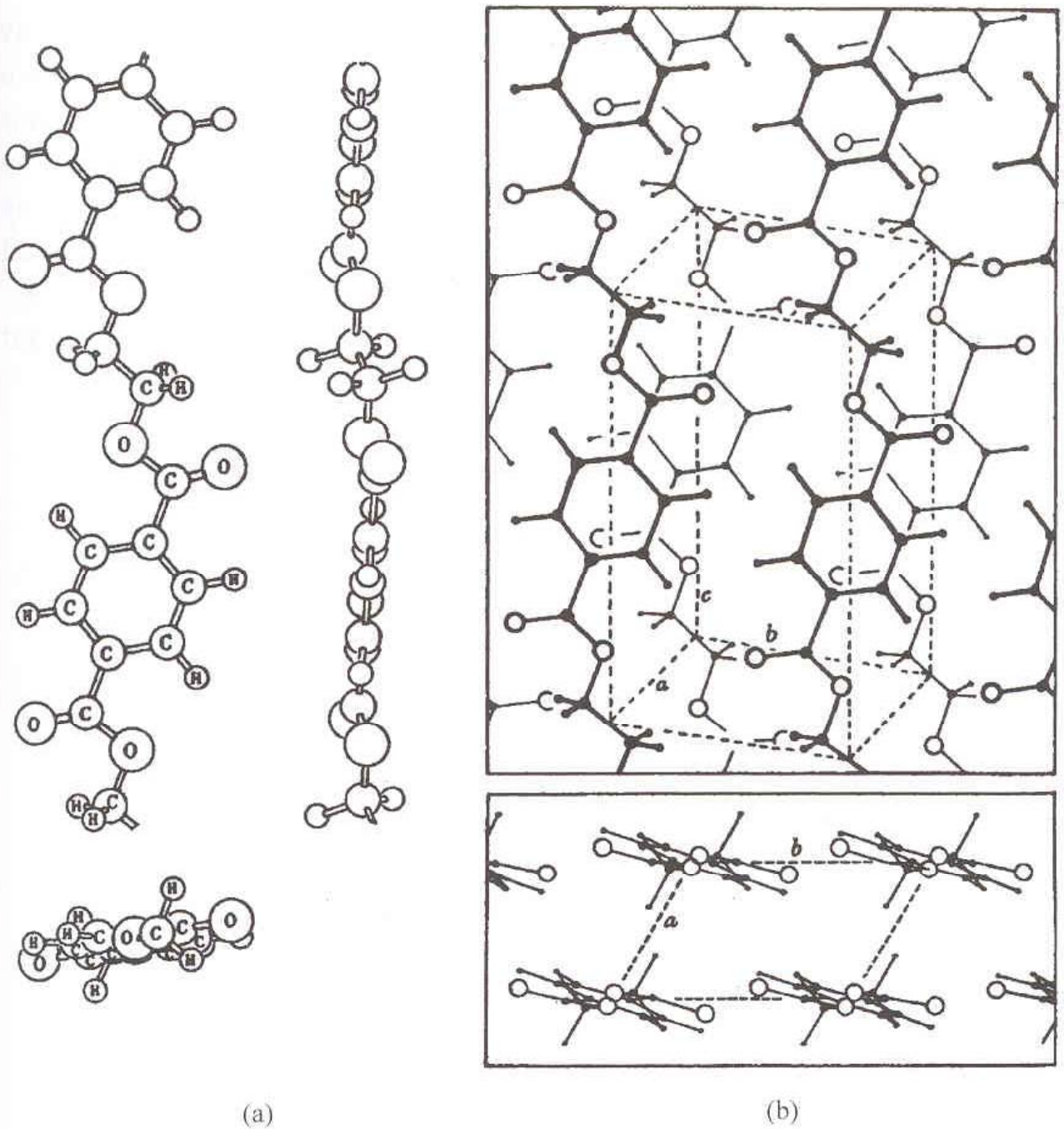

Fig. 4.19 The crystal structure of poly(ethylene terephthalate) (PET): (a) views of the chain conformation taken up in the crystal and (b) the arrangement of the chains in the crystal, with one chain passing through the triclinic unit cell. (Reproduced by permission of the Royal Society.)

Fig. 4.20 Hydrogen-bonded sheets in (a) nylon-6,6 and (b) nylon-6. The unit-cell faces are shown by the dashed lines. (Reprinted by Permission of John Wiley & Sons, Inc.)

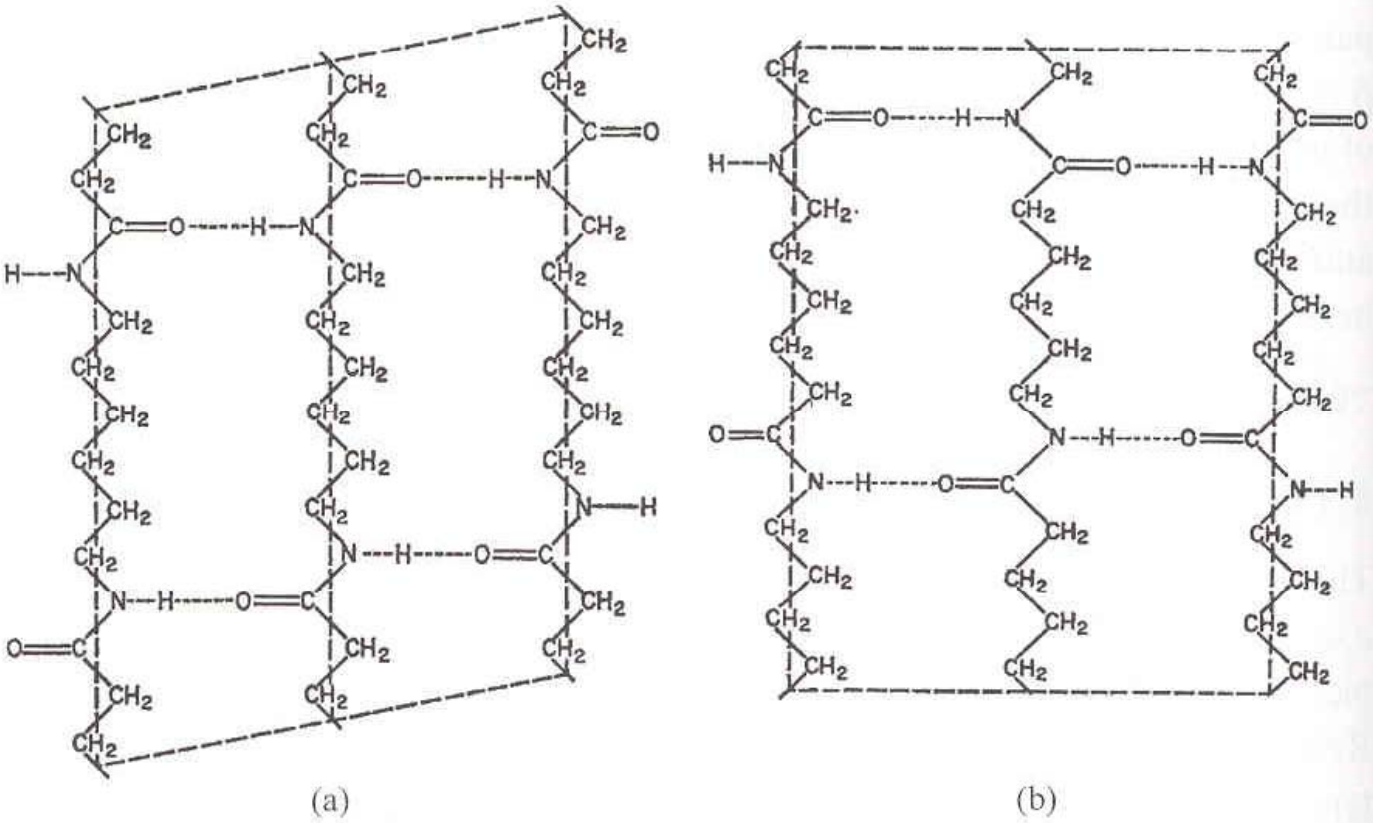

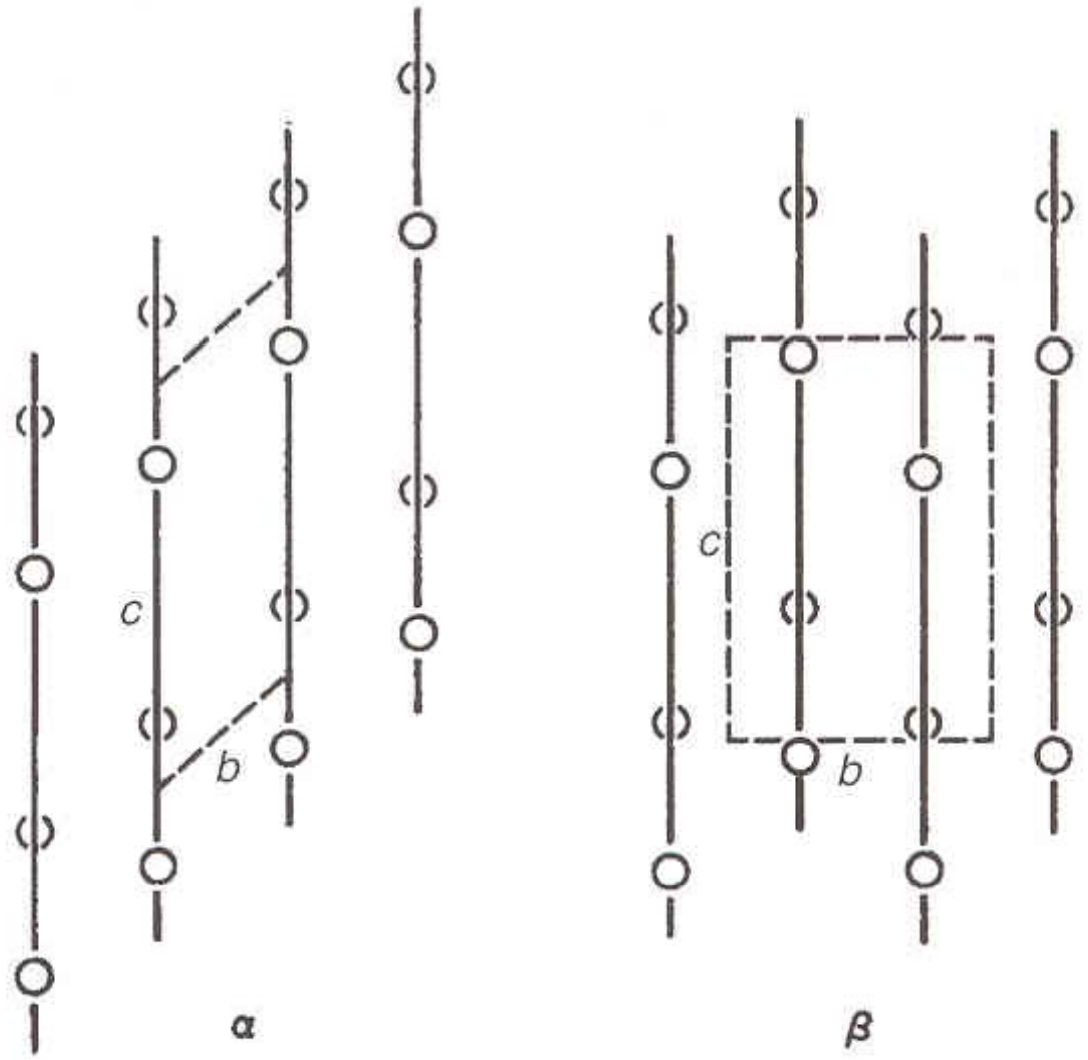

Fig. 4.21 The stacking of the hydrogen-bonded sheets in the α and β crystalline forms of nylon-6,6. The lines represent the chains and the circles the oxygen atoms. Full and broken circles represent atoms on the near and far sides of the chain, respectively. The dashed lines show the unit cell. (Reproduced by permission of the Royal Society.)

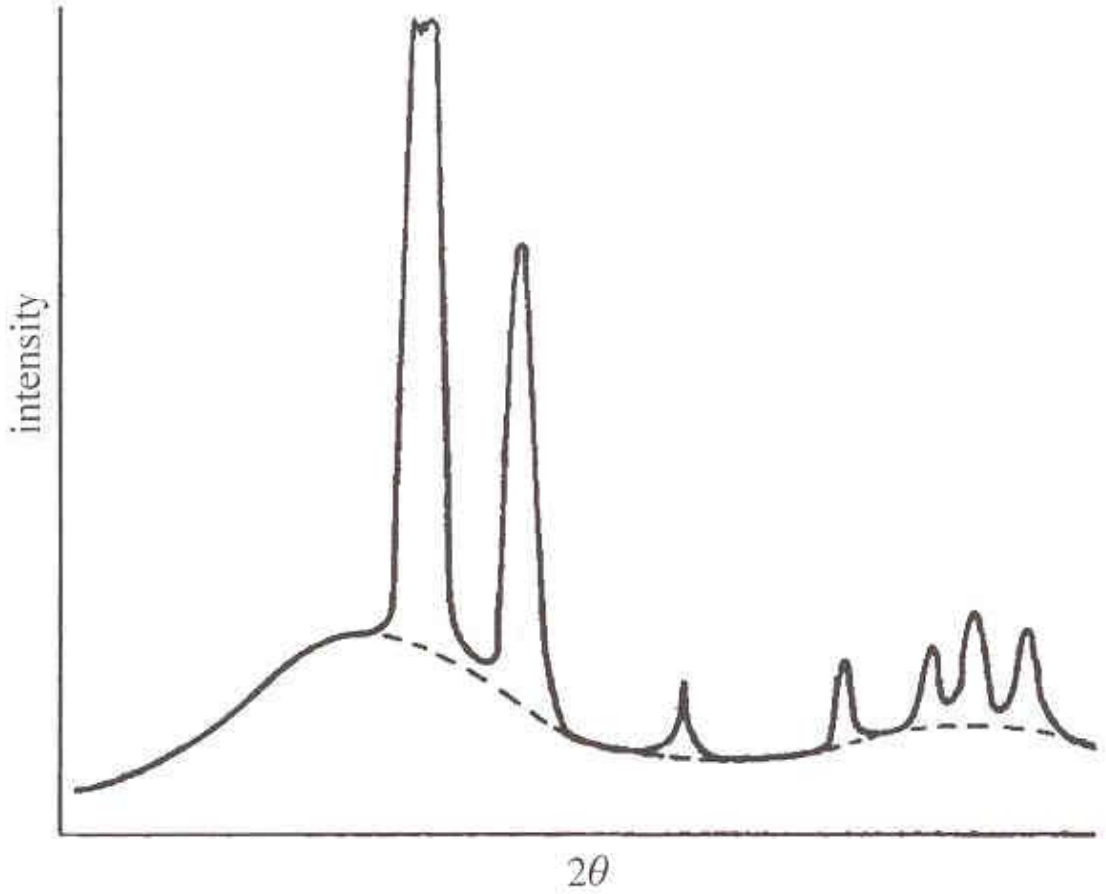

Fig. 5.1 Determination of crystallinity from X-ray scattering. The full curve shows the observed X-ray-scattering intensity as a function of 2θ, where θ is the Bragg angle and 2θ is the angle between the incident and scattered X-ray beams. The dashed curve indicates the estimated contribution of the amorphous material. (Adapted by permission of IUCr.)

Semicrystalline state

- fringed micelle model
  - intuitive and historical view
  - A chain passes through crystallites.
  - switchboard lamellar re-entry

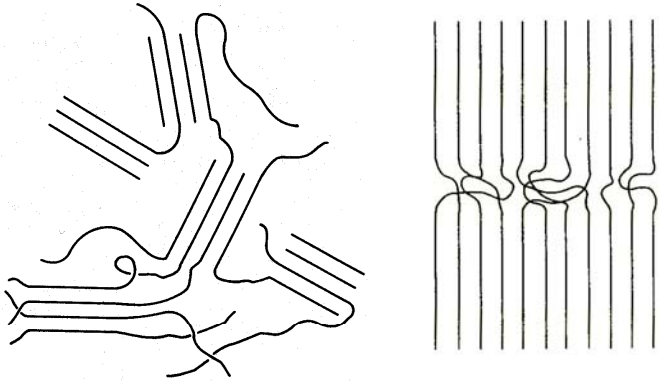

- folded chain model
  - modern view
  - suggested in single crystal lamella from dilute solution
    - Chains are perpendicular to the surface of lamella of 10-nm thick.
    - Chains got to be folded.
  - adjacent lamellar re-entry

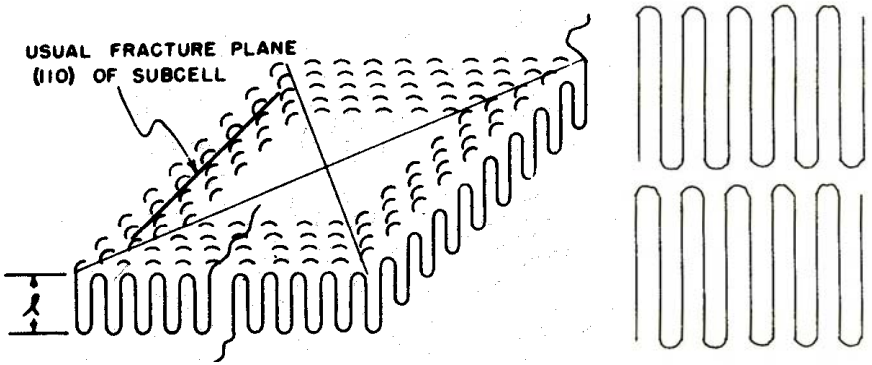

Lamella

- formed as single crystal from solution or as part of spherulite from melt

- growth of PE lamella

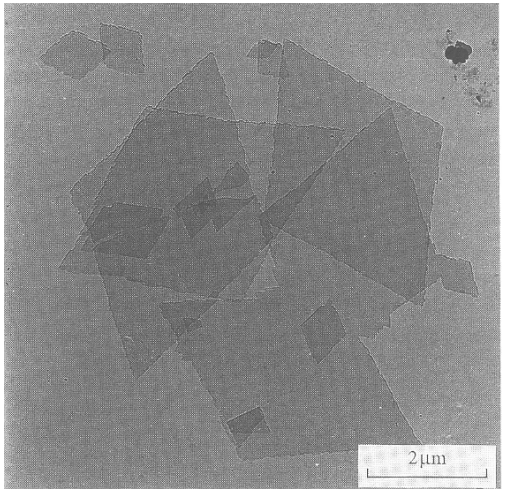

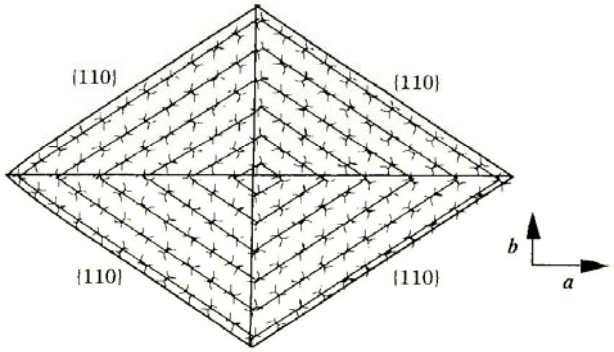

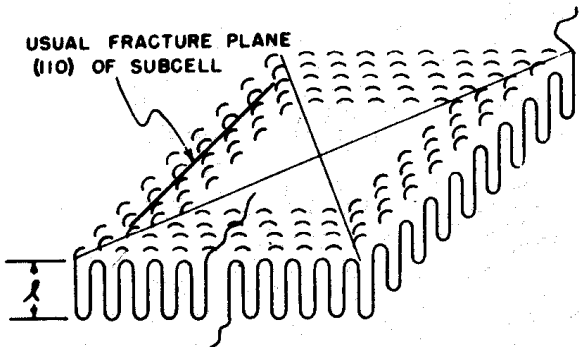

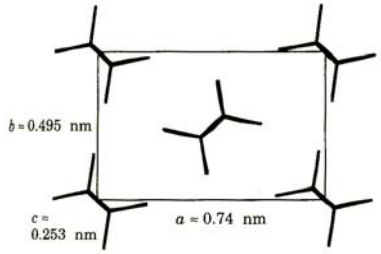

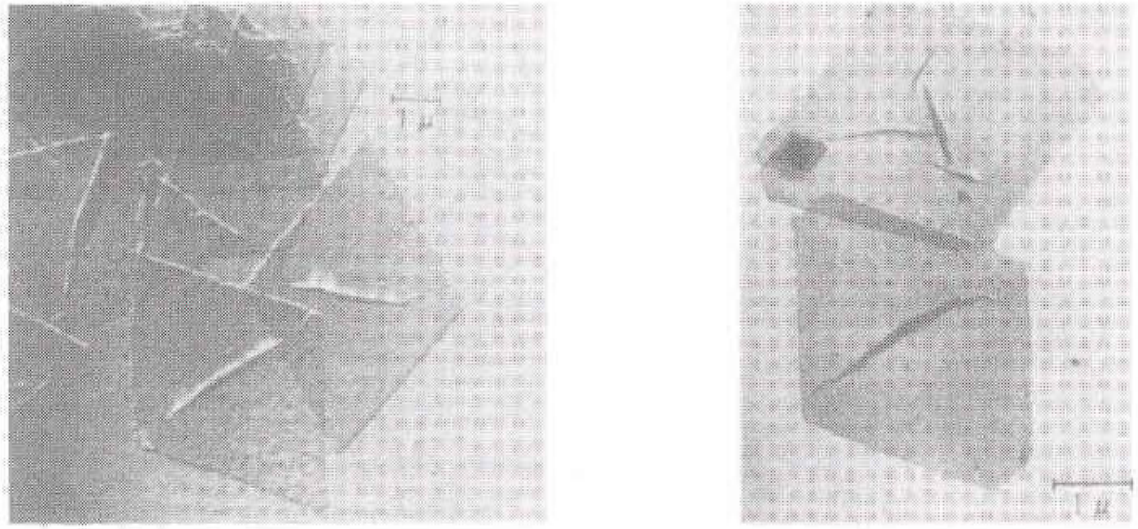

(a) (b)

Fig. 5.3 Electron micrographs of single crystals of polyethylene crystallised from dilute solution in xylene: (a) diamond-shaped crystals and (b) truncated crystals. (Reprinted by permission of John Wiley & Sons, Inc.)

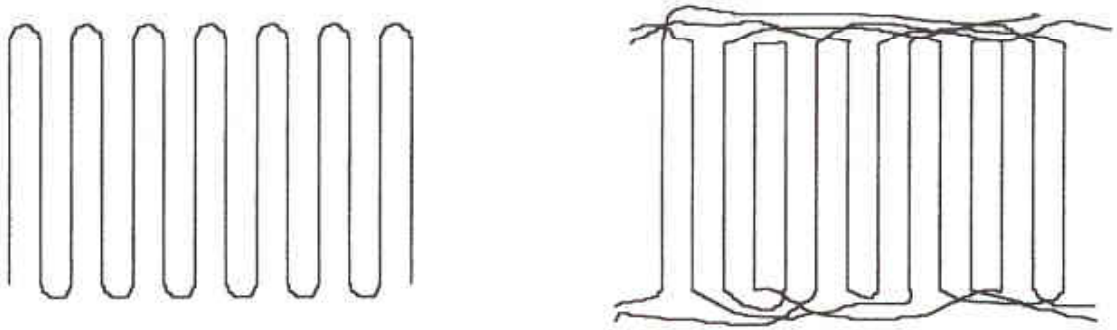

(a) (b)

Fig. 5.4 Schematic diagrams showing (a) regular chain folding with adjacent re-entry, as envisaged for a perfect chain-folded crystallite; and (b) the switchboard model.

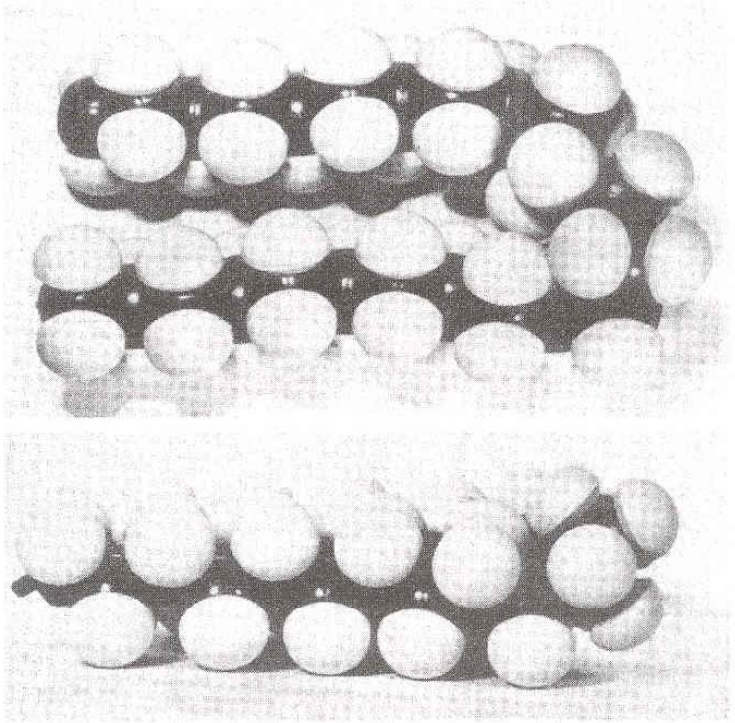

Fig. 5.6 A model of a polyethylene chain folded using four *gauche* bonds, as suggested by Frank. Upper, view normal to the plane of folding; lower, view along the plane of folding. (Reprinted by permission from John Wiley & Sons Limited.)

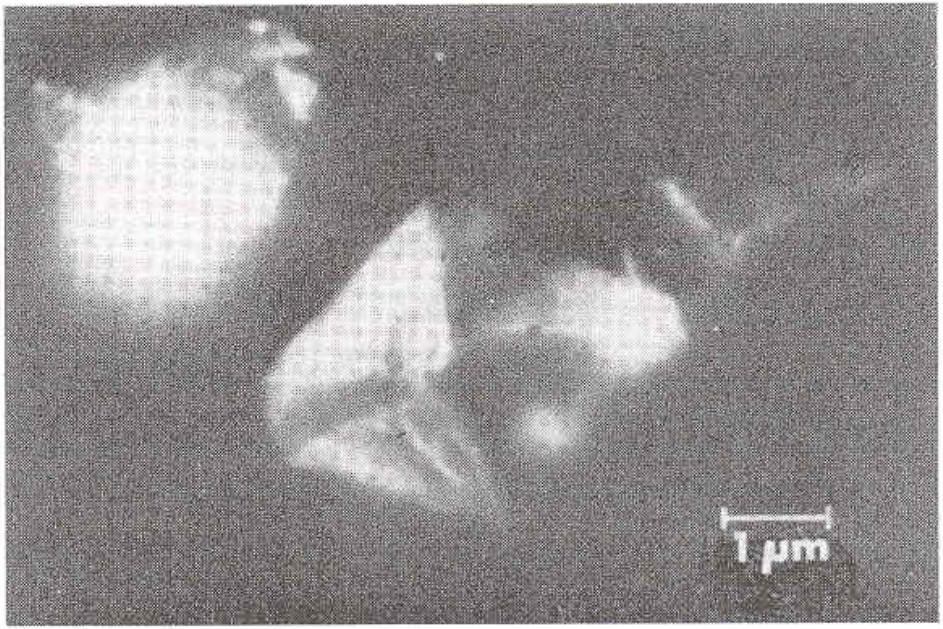

Fig. 5.5 A single crystal of polyethylene floating in solution, showing the pyramidal form. (Reprinted with permission from Elsevier Science.)

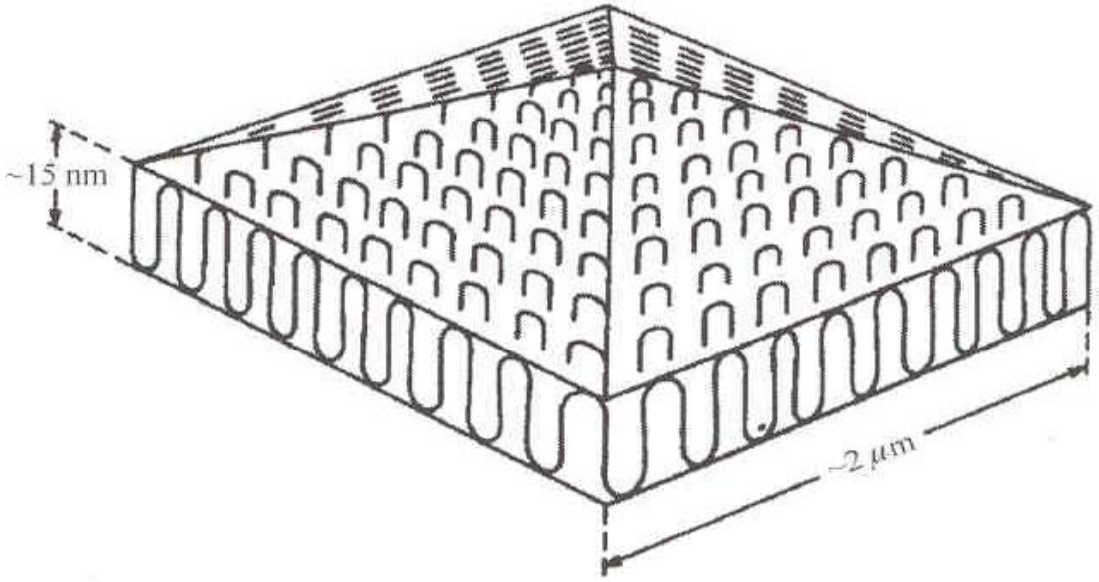

Fig. 5.8 A schematic diagram of chain folding in a solution-grown single crystal of polyethylene. (Reproduced from *The Vibrational Spectroscopy of Polymers* by D. I. Bower and W. F. Maddams. © Cambridge University Press 1989.)

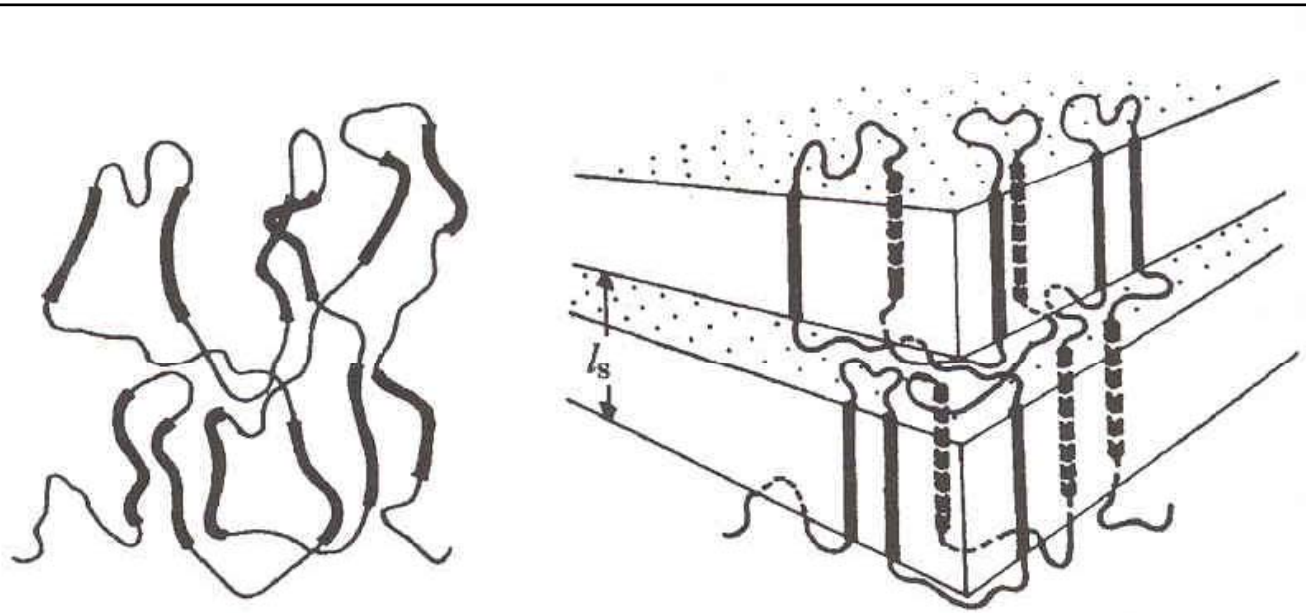

Fig. 5.7 The 'solidification model' of the crystallisation process, showing how a chain can be incorporated into a lamellar structure without significant change of overall shape. (Reproduced by permission of IUPAC.)

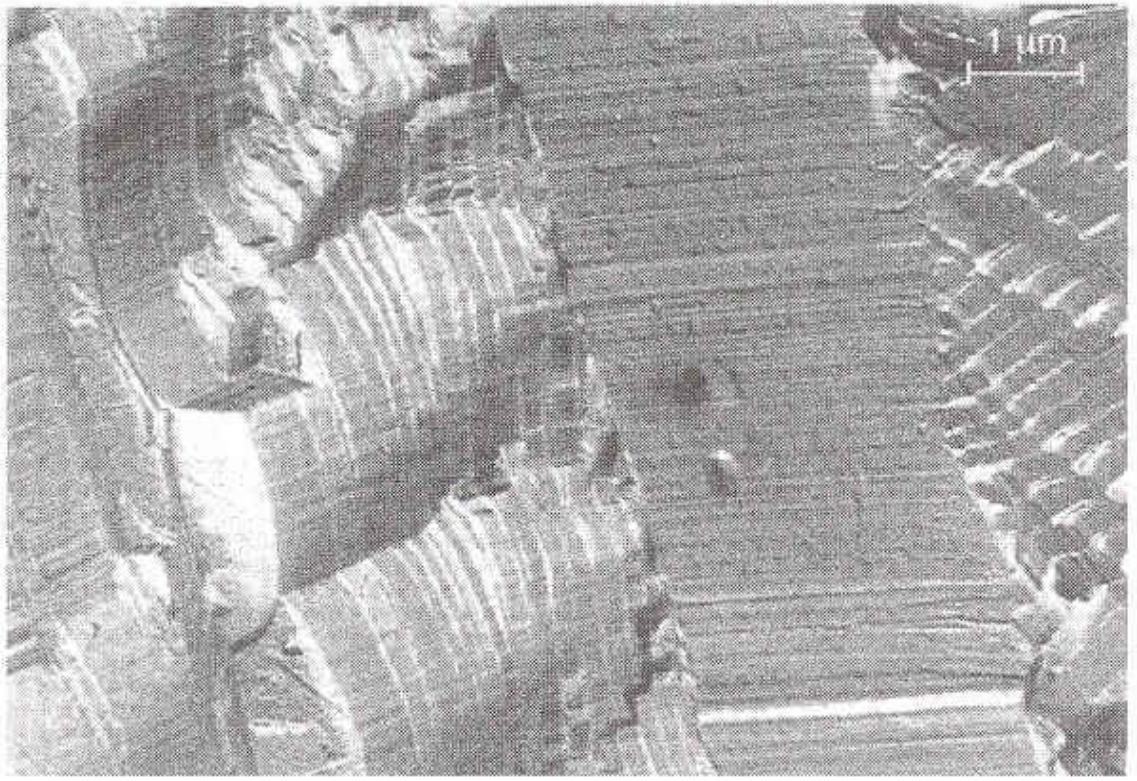

Fig. 5.9 A transmission electron micrograph of a replica of a fracture surface of extended-chain polychlorotrifluoro-ethylene. The sample was crystallised under 100 MPa pressure at 250 °C for 16 h. The sample was first heated above 295 °C. After crystallisation it was cooled rapidly to room temperature, followed by release of the pressure. (Reproduced by permission of the Society of Polymer Science, Japan.)

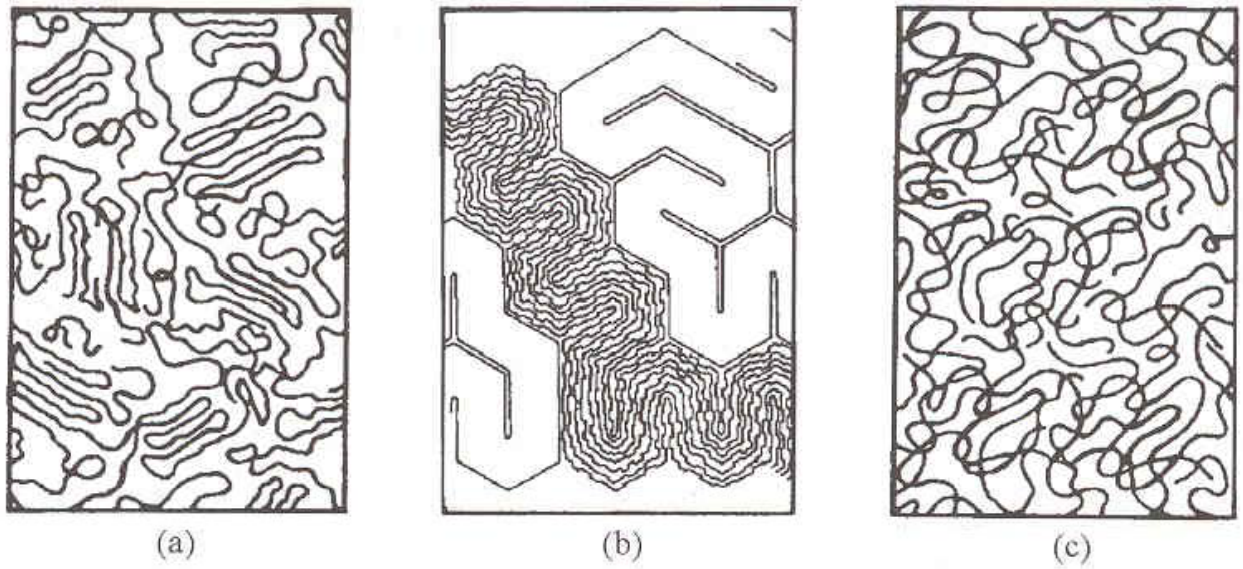

Fig. 5.10 Proposed structures for the non-crystalline regions of polymers: (a) the bundle model, (b) the meander model and (c) the random-coil model. ((a) and (c) reprinted by permission of Kluwer Academic Publishers; (b) reprinted by permission of John Wiley & Sons, Inc.)

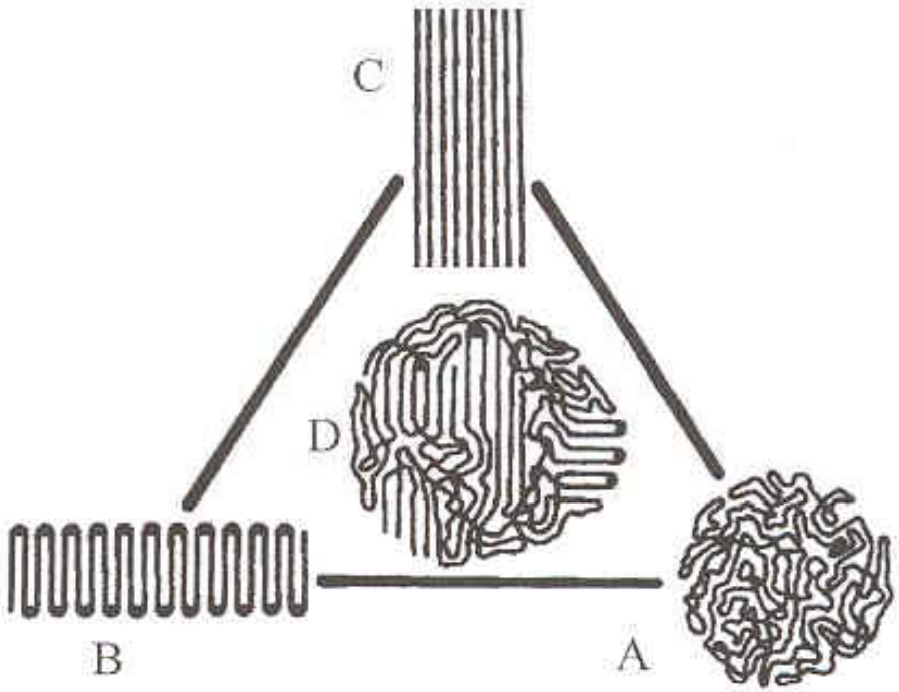

Fig. 5.11 A schematic representation of the macro-conformations of polymer chains. The vertices indicate the limiting cases. A, amorphous; B, chain-folded; C, chain-extended. The area indicates intermediate structures: D, fringed micelle. (Reproduced by permission of Academic Press.)

Spherulite

- spherical crystal from melt
  - μm – mm
- melt-crystallized
  - at high temperature → axialite (sheaf-like)
  - at low temperature → spherulite (dendritic growth)

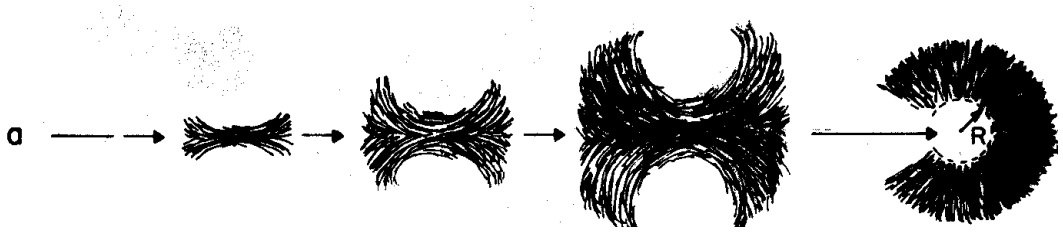

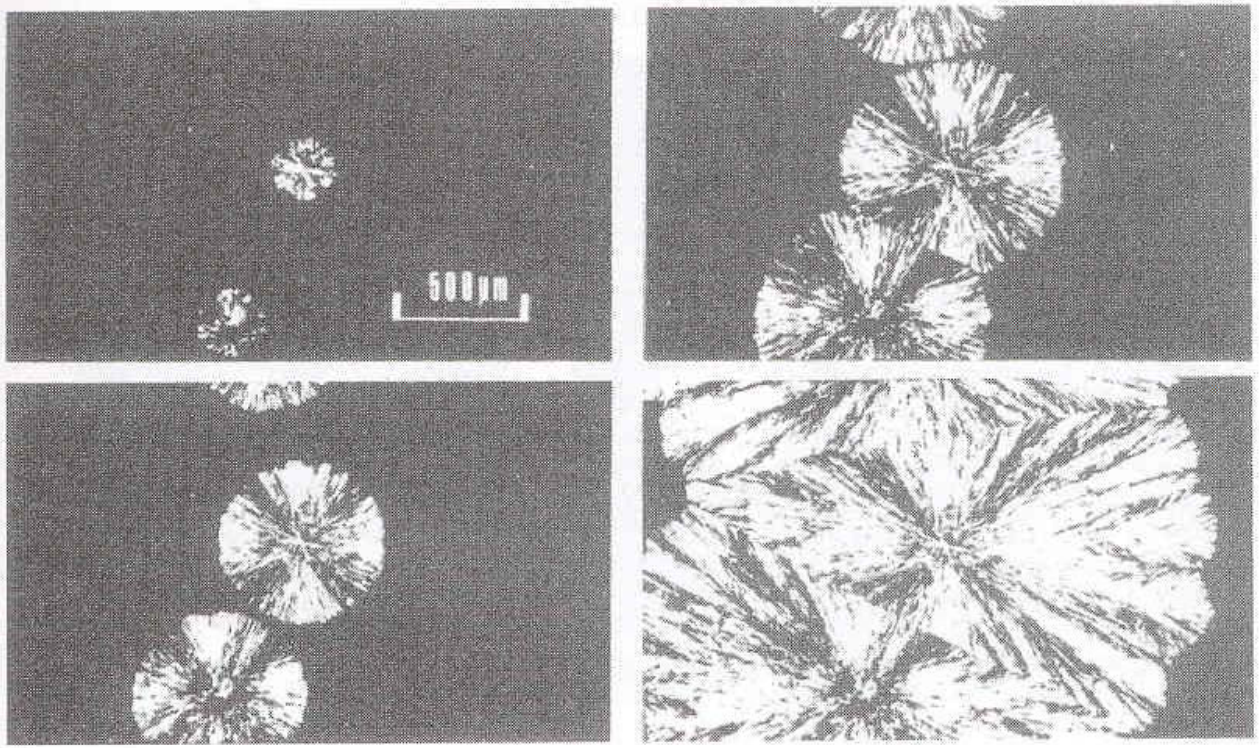

Fig. 5.13 Growth of poly(ethylene oxide) spherulites from the melt, over a period of about 1 min. The originally separate spherulites eventually impinge on each other to form an irregular matrix. (Reproduced with the permission of Nelson Thornes Ltd.)

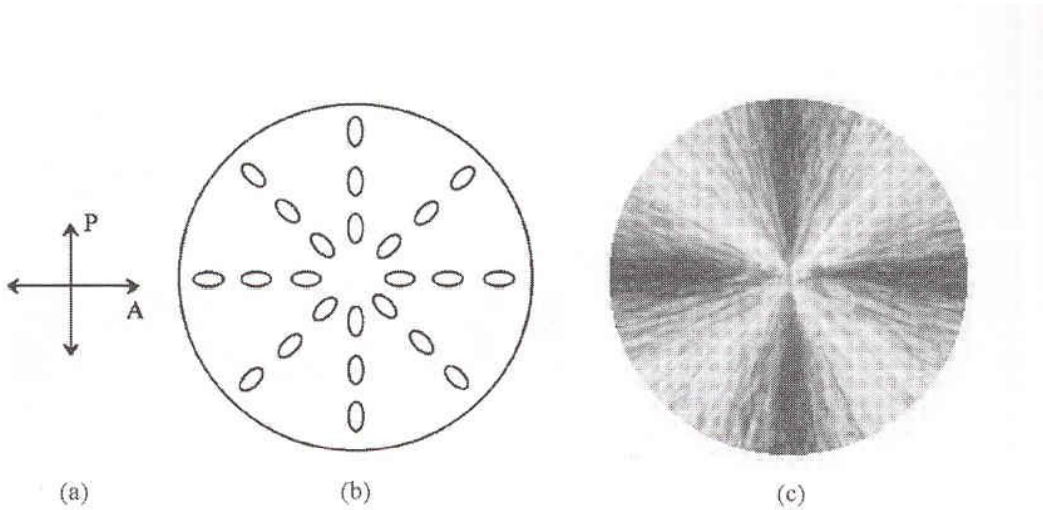

Fig. 5.14 Formation of the Maltese cross for a spherulite: (a) the directions of transmission of the polariser and analyser, (b) a schematic representation of the orientation of the indicatrices in the spherulite and (c) the appearance of the Maltese cross. In (b) the indicatrix orientations are shown for only eight radial directions, for clarity, and should be imagined for the remainder.

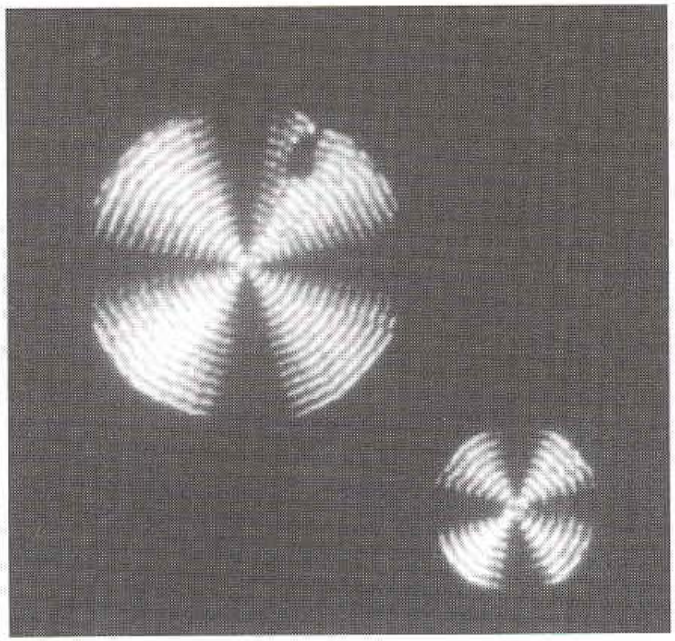

Fig. 5.15 Banded spherulites growing in a thin film of polyhydroxybutyrate. (Courtesy of Dr P. G. Klein.)

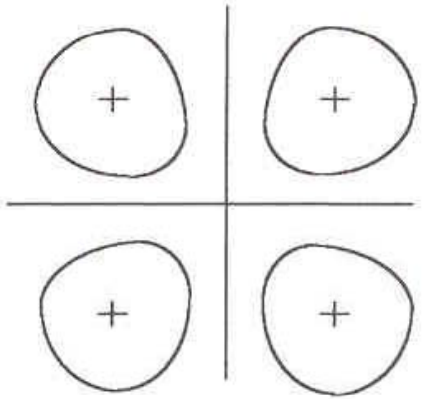

(a)

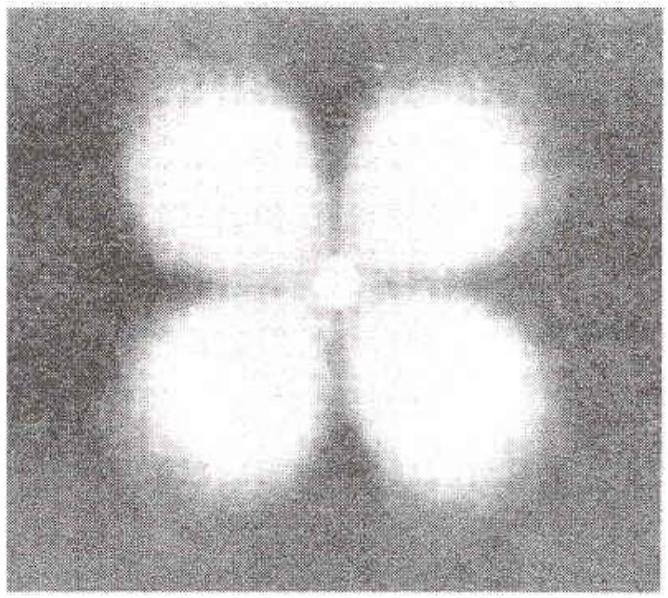

(b)

Fig. 5.16 (a) A schematic diagram of the observed light scattering from a spherulitic polymer film placed between crossed polarisers. The straight lines indicate the directions of polarisation and the closed curves indicate one contour of intensity for each of the four patches of light seen. The crosses indicate the positions of maximum intensity. (b) A photograph of the corresponding pattern for a polyethylene film. ((b) Reproduced by permission of the American Institute of Physics.)

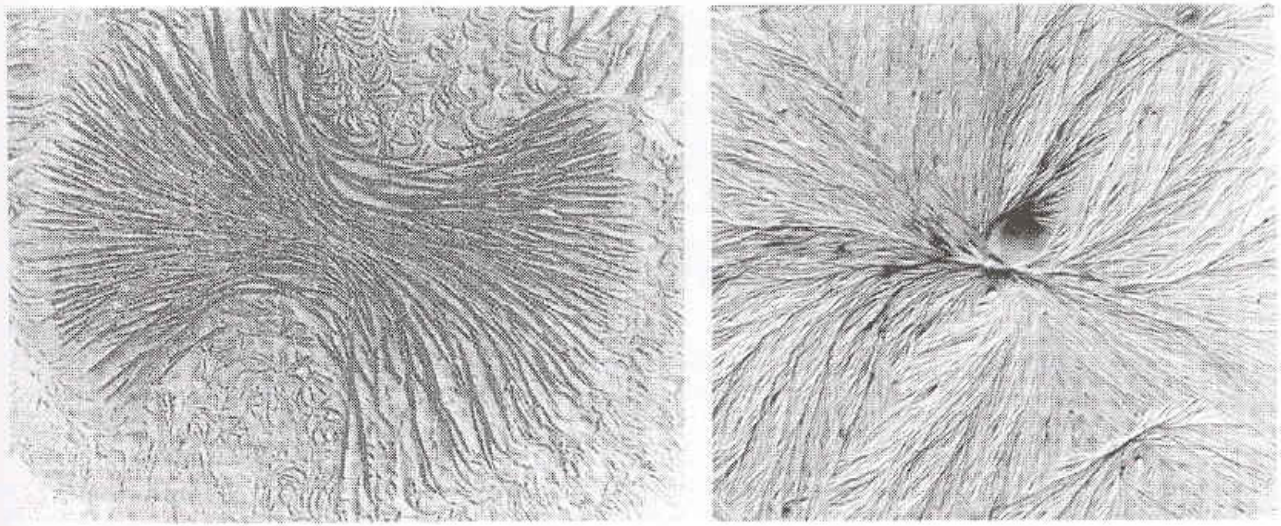

(a) (b)

Fig. 5.17 Early stages in the growth of spherulites: (a) the sheaf-life stage in the growth of a polyethylene spherulite and (b) the beginnings of radial growth in a spherulite of poly(4-methylpentane). ((a) Reprinted by permission of Kluwer Academic Publishers; (b) © Cambridge University Press 1981.)

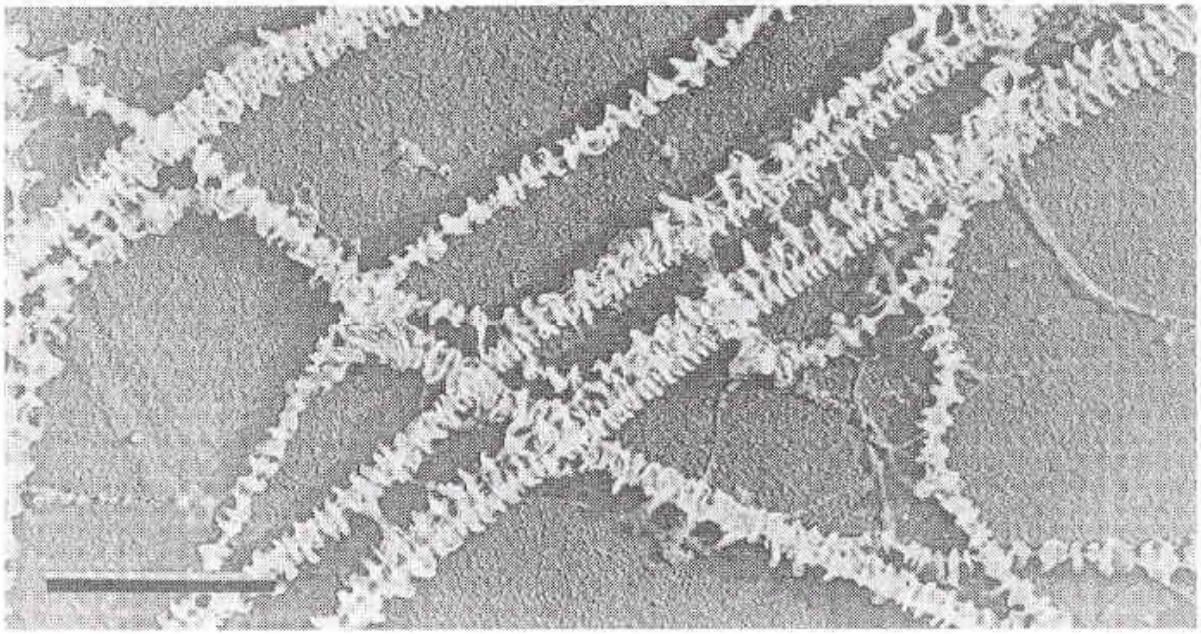

Fig. 5.18 Shish-kebab morphology produced by stirring a 5% xylene solution of polyethylene at 510 rpm and 104.5 °C; the scale bar represents 1 μm. (Adapted by permission of John Wiley & Sons, Inc.)

- radial growth
  - radius parallel to b axis
  - molecular fractionation
    - high MW first
    - low MW subsidiary or repelled
- banded spherulite
  - lamellar twisting
    - due to screw dislocation or curvature of lar

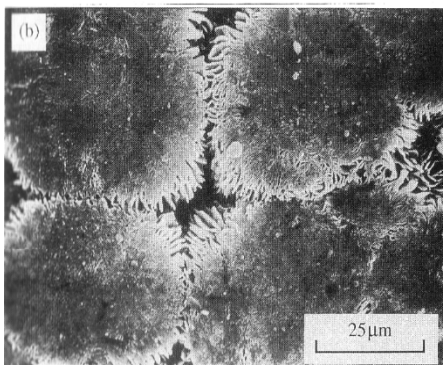

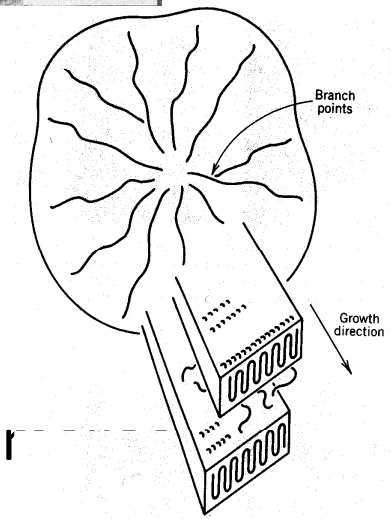

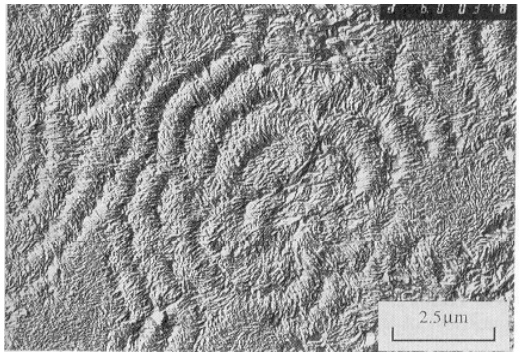

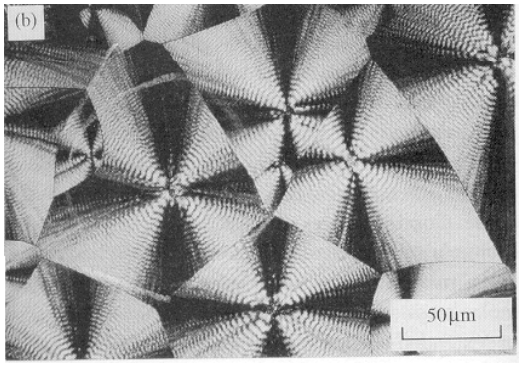

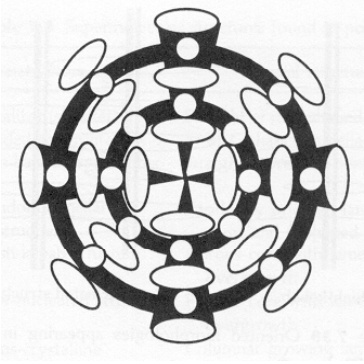

Melting of crystalline polymers

– Melting temperature of crystal

$$T_m = T_m^o \left[1 - 2\sigma / \left(l \rho_c \Delta h\right)\right]$$

– Equilibrium melting temperature

$$T_m^0 = \lim_{x \to \infty} \frac{\Delta h(x)}{\Delta s(x)}$$

- infinite MW
- Pure crystal

Size-dependent melting point of Tin

Phys. Rev. Lett. 77, 99 (1996)

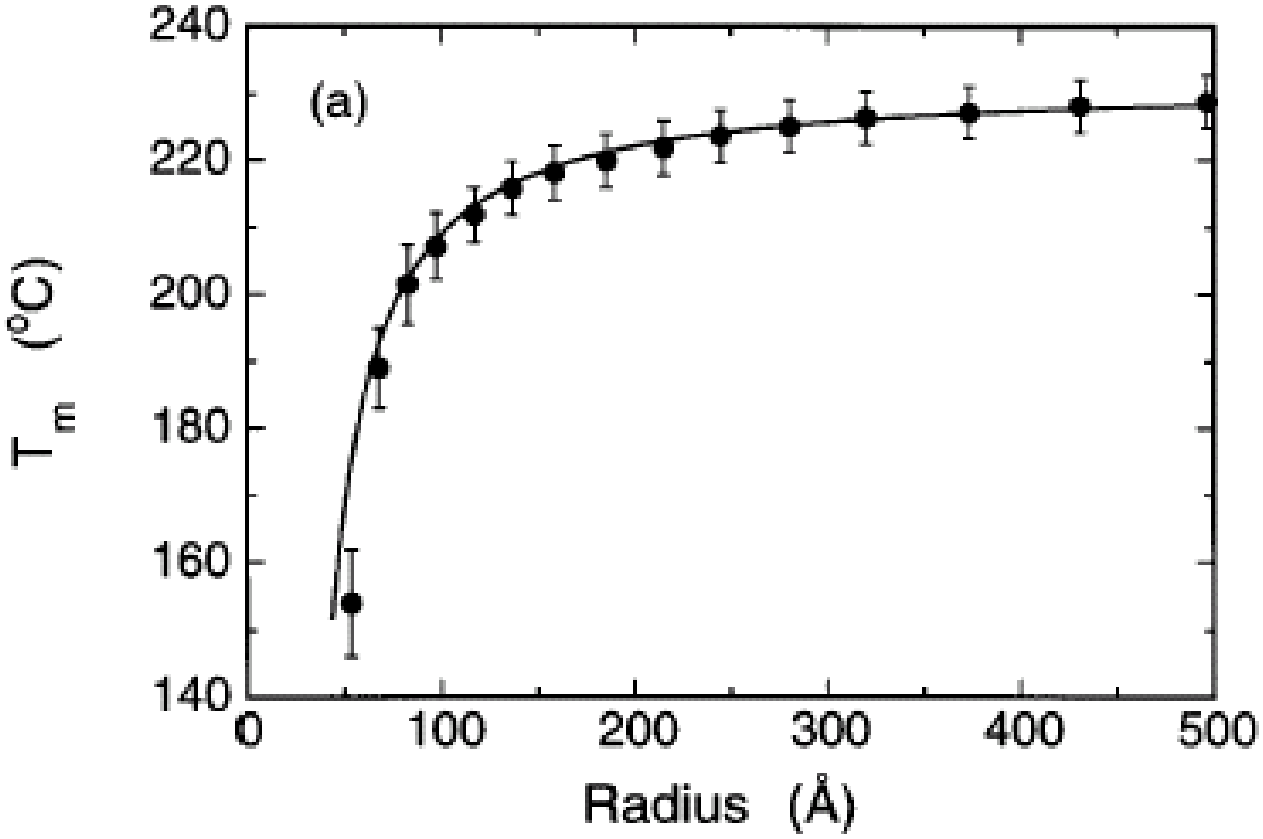

Theories for crystal growth

- equilibrium theories
  - Crystal thickness increases with T to a certain T.
  - does not predict the effect of supercooling
  - not popular

- kinetic theories
  - The end-state is not of the lowest possible energy.
  - Crystal growth rate is dep on L_c, which is determined by supercooling.

  - enthalpic nucleation theory ~ Lauritzen-Hoffman theory
  - entropic theory ~ Sadler-Gilmer theory

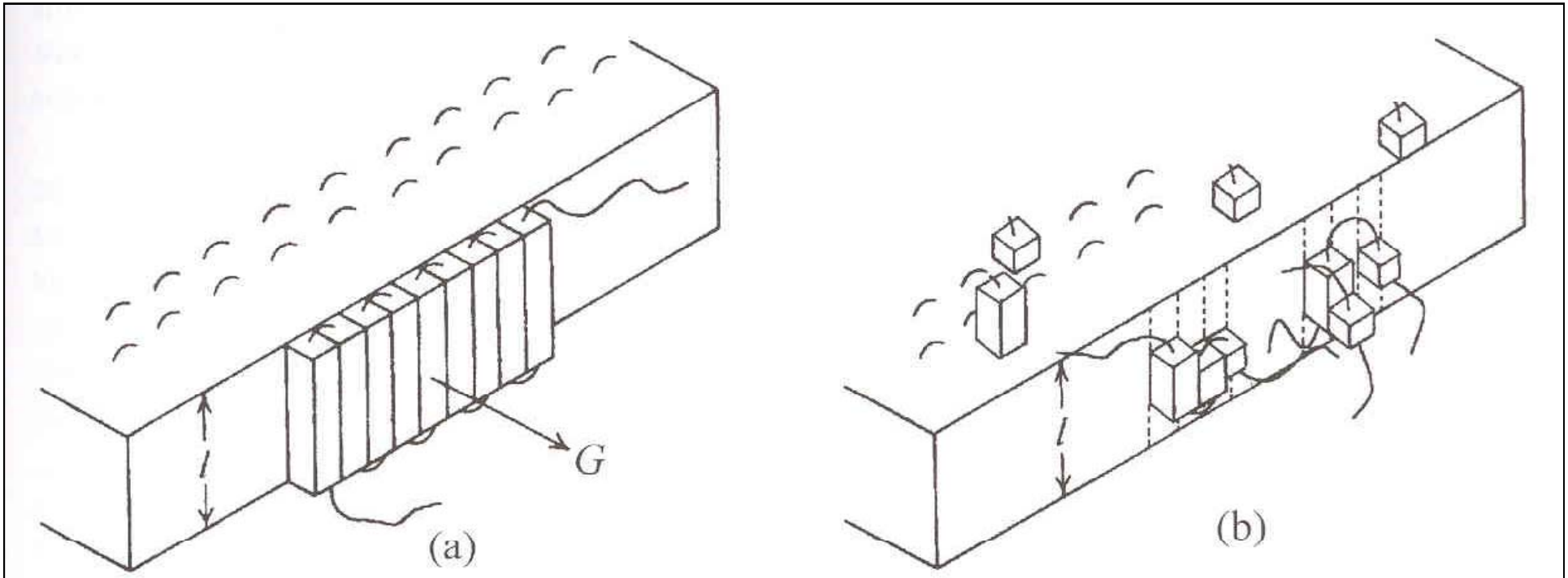

Fig. 5.19 Addition of chain segments to a growing crystallite according to (a) the Lauritzen–Hoffman theory and (b) the Sadler–Gilmer theory. Note that, in the Sadler–Gilmer theory, there are no perfectly regular fold surfaces. ((a) Adapted by permission of Kluwer Academic Publishers.)